ELECTROMAGNETIC CHARACTERIZATION OF MATERIALS USING A DUAL CHAMBERED HIGH TEMPERATURE WAVEGUIDE

THESIS

Jeffrey S. Sovern, Capt, USAF

AFIT-ENG-MS-16-M-047

DEPARTMENT OF THE AIR FORCE
AIR UNIVERSITY

AIR FORCE INSTITUTE OF TECHNOLOGY

Wright-Patterson Air Force Base, Ohio

AFIT-ENG-MS-16-M-047

ELECTROMAGNETIC CHARACTERIZATION OF MATERIALS USING A DUAL CHAMBERED HIGH TEMPERATURE WAVEGUIDE

THESIS

Presented to the Faculty

Department of Electrical and Computer Engineering

Graduate School of Engineering and Management

Air Force Institute of Technology

Air University

Air Education and Training Command

in Partial Fulfillment of the Requirements for the

Degree of Master of Science in Electrical Engineering

Jeffrey S. Sovern, B.S.

Capt, USAF

March 2016

AFIT-ENG-MS-16-M-047

ELECTROMAGNETIC CHARACTERIZATION OF MATERIALS USING A DUAL CHAMBERED HIGH TEMPERATURE WAVEGUIDE

THESIS

Jeffrey S. Sovern, B.S.
Capt, USAF

Committee Membership:

Michael J. Havrilla, PhD
Chair

Maj Milo W. Hyde, PhD
Member

Peter J. Collins, PhD
Member

AFIT-ENG-MS-16-M-047

Abstract

Measurement of the electromagnetic properties of materials at high temperatures is important for industrial, scientific, medical, and aerospace applications [1]. Current high-temperature electromagnetic material characterization is a time consuming process that typically requires three days to collect data from one material specimen. For example, the standard high-temperature process involving rectangular waveguides [2] requires measurements of the sample (1), the empty waveguide (2), and a metal short standard (3) completed in separate heated runs over three days to perform the Nicolson-Ross-Weir inversion algorithm for computing permittivity and permeability.

The technique developed here will reduce the high-temperature measurement process from three days down to just one day. The research uses a position independent approach for isotropic materials that averages forward and reverse traveling waves for effective transmission and reflection parameters. It is shown that this averaging effect eliminates the need for a metal short measurement, thus reducing high-temperature measurement time by one day. In addition, a new dual chambered waveguide design will help reduce measurement time down to just one day. This is accomplished through simultaneous measurement of the inserted sample in one of the chambers and the empty waveguide of the second chamber.

A vector network analyzer (VNA) will be used to run X-band data collects at incrementally increasing temperatures up to approximately $1000^{\circ}F$. The results will be the test material's permittivity and permeability as calculated from VNA measured S-parameters at increasing temperatures. These results will be compared with other known techniques in order to validate the new high-temperature process.

Acknowledgements

Dr. Havrilla for your guidance and knowledge. Maj Hyde for your help moving me forward. Capt Humber, without you blazing the path I would have never been here. To the good gentlemen at GE aviation for the facilities and additional insight. My fellow classmates for the camaraderie and teamwork. To TOC for the distractions; needed, helpful, and not. And to my hockey friends and family for the PT and inherent stress relief.

"Timber"

Contents

Page

List of Figures

List of Tables

ELECTROMAGNETIC CHARACTERIZATION OF MATERIALS USING A DUAL CHAMBERED HIGH TEMPERATURE WAVEGUIDE

I. Introduction

1.1 Problem Statement

The full characterization of materials in the electromagnetic (EM) spectrum is crucial when their application is in an ever-varying regime. In aerospace and defense applications, materials encounter extremes of dynamic pressure, g-forces, and of course temperature. This last condition can and does have a direct effect on the dielectric and magnetic properties of materials. Certain materials' EM properties, like polarization and permittivity, experience dramatic changes when raised above a critical temperature; this is known as the Curie point [3]. Other materials will have more subtle changes. Knowing how and when any changes will occur are critical when developing systems that interact in the radio frequency (RF) spectrum. This is when EM material characterization at high-temperatures must be performed.

High temperature EM material characterization is a time consuming process requiring three collections of data over an extended period of time. The process is time consuming due to the need to slowly increase the temperature of the furnace, wait for thermal stabilization to measure, and the ability to take only measurements on the empty, filled, or shorted waveguide, one at a time, over a full day of collection each. This process can induce error due to changing environmental effects and consistency issues between each of the three collects. The delay in collections prevents the rapid analysis of materials under test, which increases schedule and cost risks to

research and developmental programs. Additionally, the increased quantity of data collects in the harsh testing environment causes accelerated wear on the measurement apparatus, which has a limited lifetime.

1.2 Research Goals and Impact

The process developed in this thesis will reduce the typical three-day measurement time to just one day. By reducing the data collection time, material characterization analysis and material development can be accelerated. Measurement errors can be reduced through a more efficient process.

This research will take a position-independent approach for isotropic materials that will average forward and reverse travelling EM waves for effective transmission and reflection parameters. The new process will use a dual-chambered waveguide allowing two simultaneous measurements of the sample-loaded chamber and the empty chamber. The short measurement used in standard techniques will be omitted due to the averaging calculations.

With two-thirds of the time eliminated, more measurements can be run. These bonus runs can be of the same material for statistical significance, of similar materials for comparison, or re-looks to correct for initial issues discovered. This rapid development benefits the urgent needs of the defense sector and accelerates public and private research development.

1.3 Methodology

Initial runs will be accomplished at room temperature at the AFIT Microwave Laboratory to test and validate the theory and MATLAB® code before moving on to high-temperature collections. The General Electric (GE) Aviation laboratory and high-temperature clam-shell furnace are used for high-temperature collects that are

accomplished from room temperature incrementally up to $1000°F$ in the X-band using a vector network analyzer (VNA). The dual-chamber high-temperature waveguide (DCHTWG) measurements will be compared to data collected from standard material measurement techniques and error analysis using the Baker-Jarvis method [4].

1.4 Limitations and Challenges

The key limitation to all high-temperature measurements is resistance to oxidation and other degradation from the thermal effects. This is true in the test material and waveguide construction. Standard waveguides do not have the durability in the high temperature environment, thus causing the requirement for an additional waveguide inserted into the system. These high-temperature waveguides require different construction that reduce deterioration from oxidation and heat cycling. Before measuring with this inserted waveguide, careful calibrations are required to set a baseline at the end points of the additional waveguide. This adds complexity to the system, requiring flush mounting of the hardware and avoidance of any steps or gaps which could scatter the RF energy.

The isotropic assumption used in the process developed in this thesis creates unique challenges as well. The method required with this assumption prevents forward/reverse directional comparisons at high temperature. This allows homogeneity checks to be accomplished only at room temperature prior to using the DCHTWG. The additional mathematical processing created from the theory discussed in this thesis requires additional steps in MATLAB® to correct for phase.

1.5 Thesis Organization

This thesis describes the mathematical theory, development, and testing of a rapid high-temperature EM RF material characterization process. Chapter II provides

background research of material measurements including standard high-temperature procedures and mathematical development of the theory used. Chapter III addresses the baseline check of the system and theory before describing the full process of collecting high-temperature material characterization with the DCHTWG. Chapter IV displays and compares the results between baseline, traditional, and DCHTWG collects. Chapter V wraps up the research with conclusions from the analysis, discussing the effectiveness of the procedure developed here and provides recommendations for future research.

II. Background

High-temperature EM material measurement has seen numerous approaches: microwave energy for heating and measurement by M. Aral, J. G. P. Binner, G. E. Carr, and T. E. Cross [5]; free-wave and dielectrometer methods by W. W. Ho and W. R. Tinga [6, 7]; a "dual-waveguide" fixture with different inserted sample holders J. A. Batt, R. Rukus, and M. Gilden [8]; and a text chapter (12) discussing various methods in *Microwave Electronics: Measurement and Materials Characterization* [1]. These methods have inherent complexity, as broached in Chapter I, along with their impetus in aerospace and defense applications. This chapter discusses the common rectangular waveguide methods that have evolved and addresses the shortcomings that are overcome with the DCHTWG theory developed here.

This thesis theorizes, develops, and tests a streamlined process for measuring material properties at elevated temperatures. This chapter provides the history and foundation of material testing with rectangular waveguides leveraging EM theory, scattering parameters, and the extracted intrinsic properties of the material. The application of this theory is demonstrated in the process described in Chapter III.

2.1 Electromagnetic Material Property Measurement

Numerous processes [9] have been developed to measure EM properties of materials to include free-space[10], coaxial [11], strip-line [12], and rectangular waveguide [13]. Each technique has applications depending on the material and test environment. Rectangular waveguides have the advantage of precision, repeatability, and speed. These advantages bode well in high-temperature measurements also, and they contribute to the reason for choosing rectangular waveguides for the theory and process developed in this thesis.

2.1.1 Standard Rectangular Waveguide Technique.

A common process for EM material characterization is to prepare a sample of material in a cross-sectional area matching that of a rectangular waveguide and with sufficient thickness for sturdiness, while avoiding wavelength-resonant thicknesses. The material is placed in this waveguide and S-parameters are collected using a VNA that is calibrated to a standard waveguide's end, for each port. The well-documented Nicolson-Ross-Weir (NRW) algorithm [11, 14] is then used to extract the complex relative permittivity (ϵ) and permeability (μ) of the material under test.

2.1.2 Standard High-Temperature Waveguide Technique.

High temperature EM material characterization, using a single chambered waveguide inserted into the calibrated plane between two standard waveguides, is well described in Larsson and Sjöberg [2]. This closed-form solution relies on good sample location for accommodation of the phase delay. Figure 1 depicts a sample-loaded high-temperature waveguide with the length of the Port 1 half measured as length A, and the length of the Port 2 half as the sum of the thickness of the material under test, length ℓ, and length B.

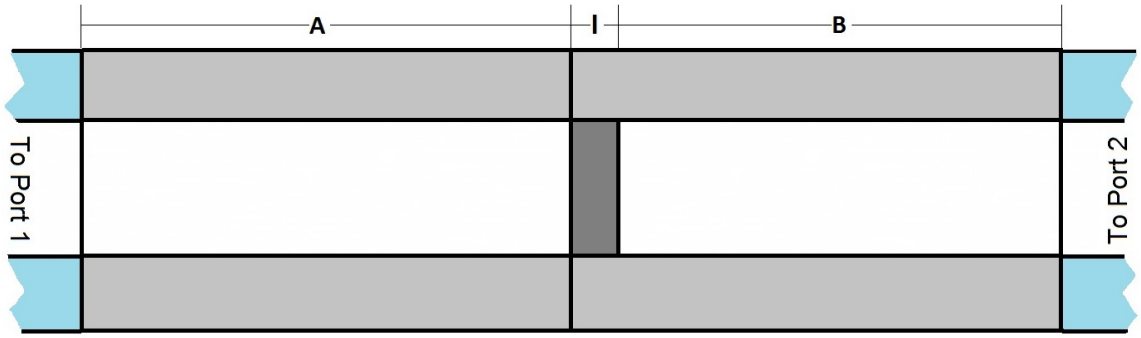

Figure 1. Sample-loaded high-temperature waveguide set-up

Equations (1a) and (1b) model the measured sample S-parameters $[S^{ms}]$ of the

reflecting waves, as they travel from their port of origin to the material in the direction of the other port [S_{12}^{A},S_{21}^{B}], reflecting off the material under test (sample) [S_{11}^{s},S_{22}^{s}], and then back to the the originating port [S_{21}^{A},S_{12}^{B}]. These equations are then rearranged to isolate the sample's experimental S-parameters [S^{s}]. Similarly, equations (1c) and (1d) model the S^{ms} of the transmitted waves through waveguide section A, the sample, and waveguide section B to the opposite port. Again, the equations are rearranged to isolate S^{s}.

$$S_{11}^{ms} = S_{21}^{A} S_{11}^{s} S_{12}^{A} \;\Rightarrow\; S_{11}^{s} = \frac{S_{11}^{ms}}{S_{21}^{A} S_{12}^{A}} \tag{1a}$$

$$S_{22}^{ms} = S_{12}^{B} S_{22}^{s} S_{21}^{B} \;\Rightarrow\; S_{22}^{s} = \frac{S_{22}^{ms}}{S_{12}^{B} S_{21}^{B}} \tag{1b}$$

$$S_{21}^{ms} = S_{21}^{A} S_{21}^{s} S_{21}^{B} \;\Rightarrow\; S_{21}^{s} = \frac{S_{21}^{ms}}{S_{21}^{A} S_{21}^{B}} \tag{1c}$$

$$S_{12}^{ms} = S_{12}^{B} S_{12}^{s} S_{12}^{A} \;\Rightarrow\; S_{12}^{s} = \frac{S_{12}^{ms}}{S_{12}^{B} S_{12}^{A}} \tag{1d}$$

The short measurement places a perfectly electric-conducting metallic standard between the two halves as shown in Figure 2, in order to find the phase delay for the reflected waves. Equation (2) provides the mathematical models for the reflection (2a)

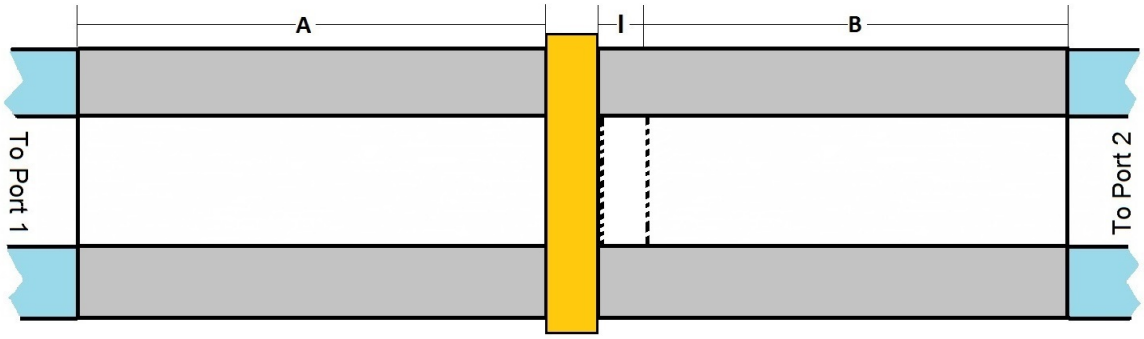

Figure 2. Shorted high-temperature waveguide set-up

from the standard and the delay, through a depth of air equivalent to the thickness

of the sample, or the empty measurement (2b).

$$S_{11}^{sh} = -1 = S_{22}^{sh} \tag{2a}$$

$$S_{12}^{e} = e^{-jk_{z_0}\ell} = S_{21}^{e} \tag{2b}$$

Equations (3a) and (3c) both rearrange the linear measured short model to isolate the product of the forward and reverse traveling waves, $S_{21}^{x}S_{12}^{x}$, using the given relations from (2) for variable elimination. Substituting these results into Equations (1a) and (1b) then provides the measured sample to measured short ratios in Equations (3b) and (3d) that give the sample reflected S-parameters.

$$S_{11}^{msh} = S_{21}^{A}S_{11}^{sh}S_{12}^{A} \;\Rightarrow\; S_{21}^{A}S_{12}^{A} = \frac{S_{11}^{msh}}{S_{11}^{sh}} = \frac{S_{11}^{msh}}{-1} = -S_{11}^{msh} \tag{3a}$$

$$S_{11}^{s} = \frac{S_{11}^{ms}}{-S_{11}^{msh}} \tag{3b}$$

$$S_{22}^{msh} = S_{12}^{B}S_{12}^{e}S_{22}^{sh}S_{21}^{e}S_{21}^{B} \;\Rightarrow\; S_{12}^{B}S_{21}^{B} = \frac{S_{22}^{msh}}{S_{12}^{e}S_{21}^{e}S_{22}^{sh}} = -S_{22}^{msh}e^{j2k_{z_0}\ell} \tag{3c}$$

$$S_{22}^{s} = \frac{S_{22}^{ms}}{-S_{22}^{msh}e^{j2k_{z_0}\ell}} \tag{3d}$$

The last measurement is of the empty waveguide, show in Figure 3, in order to find the phase delay of the wave traveling through the sample. The relations in (4a)

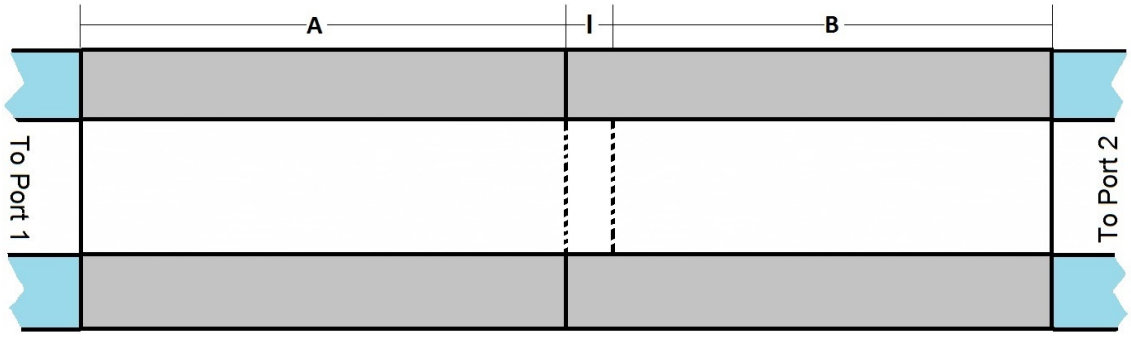

Figure 3. Empty high-temperature waveguide set-up

and (4c) isolate the measured empty value from the product of the transmitted waves, and take the given values from (2) again for variable elimination. The relations, of $S_{21}^A S_{21}^B = S_{21}^{me} e^{jk_{z0}\ell}$ and $S_{12}^B S_{12}^A = S_{12}^{me} e^{jk_{z0}\ell}$, can then be substituted into the forward (1c) and reverse (1d) traveling measured sample equations to provide a solution for the sample forward (4b) and reverse (4d) transmitted S-parameters.

$$S_{21}^{me} = S_{21}^A S_{21}^e S_{21}^B \Rightarrow S_{21}^A S_{21}^B = \frac{S_{21}^{me}}{S_{21}^e} = \frac{S_{21}^{me}}{e^{-jk_{z0}\ell}} = S_{21}^{me} e^{jk_{z0}\ell} \tag{4a}$$

$$S_{21}^s = \frac{S_{21}^{ms}}{S_{21}^{me} e^{jk_{z0}\ell}} \tag{4b}$$

$$S_{12}^{me} = S_{12}^B S_{12}^e S_{12}^A \Rightarrow S_{12}^B S_{12}^A = \frac{S_{21}^{me}}{S_{21}^e} = \frac{S_{12}^{me}}{e^{-jk_{z0}\ell}} = S_{12}^{me} e^{jk_{z0}\ell} \tag{4c}$$

$$S_{12}^s = \frac{S_{12}^{ms}}{S_{12}^{me} e^{jk_{z0}\ell}} \tag{4d}$$

With all four S-parameters, the forward and reverse complex ϵ and μ of the material under test can be calculated using the NRW [11, 14] algorithm, as accomplished for room temperature.

2.2 Dual-Chamber High-Temperature Waveguide Measurement

Common high-temperature waveguide measurement concerns are additional phase delays along the waveguide, due to thermal expansion, and sample location shift along the waveguide. These concerns are addressed by the calibration and position independence inherent in the process developed here. Assuming the material is isotropic and directionally independent allows the assumption that forward and reverse waves will act similarly and can be averaged to provide a reliable value. This does remove the quality control that having both the forward and reverse data provide, which must be compensated with proper preparation and attention to detail. The solution is open-formed and requires a root search (accomplished here) or an initial hypoth-

esis. This process was developed concurrently between this thesis and a conference presentation [15]. The following subsections elaborate on the details presented.

2.2.1 DCHTWG Position Independent Theory.

The DCHTWG is set up similarly to standard room-temperature sample holders and standard high-temperature waveguides. The two chambers allow simultaneous measurement of the empty and sample-loaded sections as shown in Figure 4. The chambers are machined to the exact same size to each other for the frequency band measured and are interchangeable. Measurements can be collected using a single 4-port VNA. Without a 4-port VNA, two 2-port VNAs can collect the measurements—provided careful calibrations are accomplished.

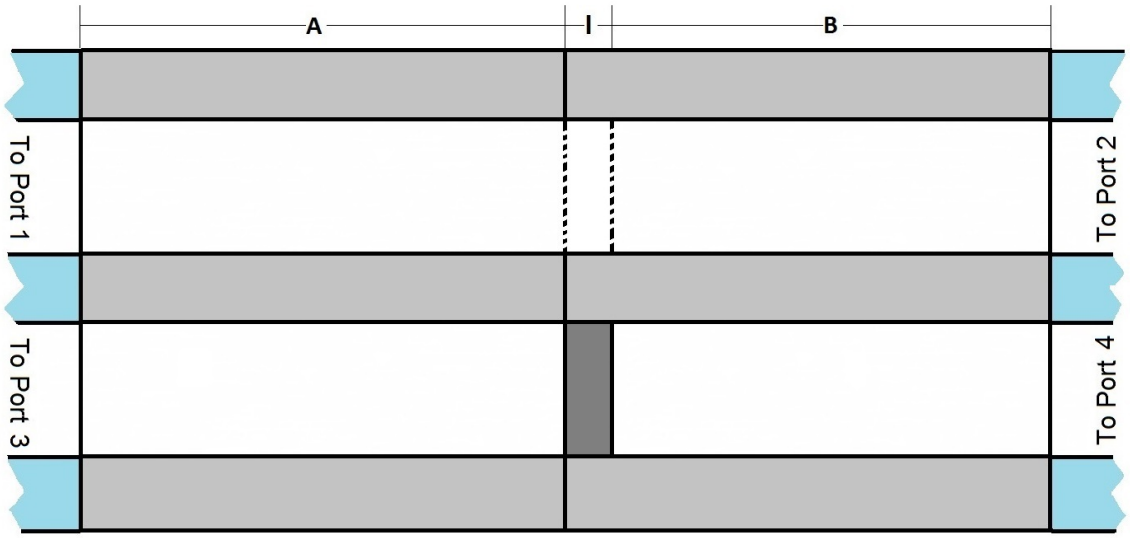

Figure 4. Sample-loaded DCHTWG set-up

The position independence is gained with the product of (1a) and (1b) in (5a). Any offset of the sample location on the A side is offset by the same and opposite delta on the B side, when they are combined in the denominator. Swapping the denominators in (5b) to pair the forward traveling waves with the Port 1 side reflection

and the reverse traveling waves with the Port 2 side reflection set-up the next substitution of (4b) and (4d) in the denominators of Equation (5c). Combining the air gap measurements to the second denominator in (5d) isolate the nominal reflected S-parameters. Repeating the same process for the transmitted waves results in (5e).

$$S_{11}^s S_{22}^s = \frac{S_{11}^{ms}}{S_{21}^A S_{12}^A} \frac{S_{22}^{ms}}{S_{12}^B S_{21}^B} = \dots \tag{5a}$$

$$\frac{S_{11}^{ms}}{S_{21}^A S_{21}^B} \frac{S_{22}^{ms}}{S_{12}^B S_{12}^A} = \dots \tag{5b}$$

$$\frac{S_{11}^{ms}}{S_{21}^{me} e^{jk_{z_0}\ell}} \frac{S_{22}^{ms}}{S_{12}^{me} e^{jk_{z_0}\ell}} = \dots \tag{5c}$$

$$\frac{S_{11}^{ms}}{S_{21}^{me}} \frac{S_{22}^{ms}}{S_{12}^{me} e^{j2k_{z_0}\ell}} = S_{11}^N S_{22}^N \tag{5d}$$

$$S_{21}^s S_{12}^s = \frac{S_{21}^{ms}}{S_{12}^{me}} \frac{S_{21}^{ms}}{S_{12}^{me} e^{j2k_{z_0}\ell}} \tag{5e}$$

The theory must be applied through correctly combining the magnitudes and phases, as shown in (6).

$$S_{11}^s S_{22}^s = \frac{S_{11}^{ms}}{S_{21}^{me}} \frac{S_{22}^{ms}}{S_{12}^{me} e^{j2k_{z_0}\ell}} = \left|\frac{S_{11}^{ms}}{S_{21}^{me}}\right| \left|\frac{S_{22}^{ms}}{S_{12}^{me}}\right| \; exp[j(\angle \frac{S_{11}^{ms}}{S_{21}^{me}} + \angle \frac{S_{22}^{ms}}{S_{12}^{me}} e^{-j2k_{z_0}\ell})] \tag{6a}$$

$$S_{21}^s S_{12}^s = \frac{S_{21}^{ms}}{S_{21}^{me}} \frac{S_{12}^{ms}}{S_{12}^{me} e^{j2k_{z_0}\ell}} = \left|\frac{S_{21}^{ms}}{S_{21}^{me}}\right| \left|\frac{S_{12}^{ms}}{S_{12}^{me}}\right| \; exp[j(\angle \frac{S_{21}^{ms}}{S_{21}^{me}} + \angle \frac{S_{12}^{ms}}{S_{12}^{me}} e^{-j2k_{z_0}\ell})] \tag{6b}$$

An extra check is required to ensure the correct inverse tangent branch cut is taken when extracting the angles from the measurements. To accomplish this an unwrapping function is performed during (6) on the angle calculations. It is possible to get a π radian shift if the two summed angles lie on both sides of the branch cut (-0.99π and 0.99π) if this check is not performed. The MATLAB® function "unwrap" was used in this research. These nominal S-parameters can now be processed to extract the material properties.

2.2.2 DCHTWG Material Property Extraction.

The effective reflected S-parameter is a geometric mean value of the two reflected S-parameters, shown as the square-root of the product of the reflected S-parameters in (7a); paralleled by the transmitted S-parameters in (7b).

$$S_{11}^{eff} = \sqrt{S_{11}^{s} S_{22}^{s}} \tag{7a}$$

$$S_{21}^{eff} = \sqrt{S_{21}^{s} S_{12}^{s}} \tag{7b}$$

The well known NRW algorithms [11, 14] start with the reflected (8a) and transmitted (8b) scattering parameters in the form of the interfacial reflection coefficient, R, and the one-way phase attenuation or propagation coefficient, P.

$$S_{11}^{eff} = \frac{R(1-P^2)}{1-R^2P^2} \tag{8a}$$

$$S_{21}^{eff} = \frac{P(1-R^2)}{1-R^2P^2} \tag{8b}$$

To accomplish a closed-form inverse solution, the S-parameters, (8), are rearranged to solve for P^2 and P, (9a) and (9b), then combined to have the propagation coefficient as a function of the reflection coefficient and the transmitted and reflected S-parameters, (9c).

$$P^2 = \frac{R - S_{11}^{eff}}{R(1 - RS_{11}^{eff})} \tag{9a}$$

$$P = \frac{S_{21}^{eff}(1-R^2P^2)}{1-R^2} \tag{9b}$$

$$P = \frac{S_{21}^{eff}}{1 - R\ S_{11}^{eff}} \tag{9c}$$

Setting (9a) and the square of (9c) equal to each other eliminates the propagation coefficient to provide a relation between the S-parameters and the reflection coefficient,

(10).

$$\frac{R - S_{11}^{eff}}{R(1 - RS_{11}^{eff})} = \left(\frac{S_{21}^{eff}}{1 - R^2 S_{11}^{eff}}\right)^2 \Rightarrow \frac{R - S_{11}^{eff}}{R} = \frac{\left(S_{21}^{eff}\right)^2}{1 - R^2 S_{11}^{eff}} \tag{10}$$

With this relation rearranged to resolve the reflection coefficient, (11a), as a function of the effective S-parameters, simplified as the quadratic solution, Q, (11b) the closed-form solution for R can be resolved, (11c).

$$R^2 - 2QR + 1 = 0 \tag{11a}$$

$$Q = \frac{(S_{11}^{eff})^2 - (S_{21}^{eff})^2 + 1}{2S_{11}^{eff}} \tag{11b}$$

$$R = Q \pm \sqrt{Q^2 + 1} \tag{11c}$$

The reflection coefficient must have a magnitude less than one for a passive material. The two choices available from (11c) are $R_1 = Q + \sqrt{Q^2 - 1}$ and $R_2 = Q - \sqrt{Q^2 - 1}$. The relationship between the two results is shown in (12) with a convenient conjugate cancellation.

$$R_1 = Q + \sqrt{Q^2 - 1} = \frac{Q + \sqrt{Q^2 - 1}}{1}\frac{Q - \sqrt{Q^2 - 1}}{Q - \sqrt{Q^2 - 1}} = \frac{1}{Q - \sqrt{Q^2 - 1}} = \frac{1}{R_2} \tag{12}$$

With this simple relation a root test is accomplished where, if condition (13a) is met, then routine (13b) is performed to meet the passive material requirement.

$$|R| > 1 \tag{13a}$$

$$R = \frac{1}{R} \tag{13b}$$

The reflection and propagation constants can be presented in terms of material properties, (14a) & (14c), to connect material measurements and properties towards the final material characterization. The material's normalized wave impedance, z,

(14b) and the material's wave number, k_z, (14d) are then calculated with the material's reflection, R, (11c) and propagation, P, (9c) coefficients from the measurements.

$$R = \frac{Z - Z_0}{Z + Z_0} = \frac{z - 1}{z + 1}\ ,\ z = \frac{Z}{Z_0} \tag{14a}$$

$$z = \frac{1 + R}{1 - R} \tag{14b}$$

$$P = e^{-jk_z\ell} \tag{14c}$$

$$k_z = \frac{\jmath\ ln(P)}{\ell} \tag{14d}$$

The complex relative permeability (15b) can then be withdrawn from the wavenumbers (k_z& k_{z_0}) and material impedance (z), (15a).

$$z = \frac{Z}{Z_0} = \frac{\omega\mu/k_z}{\omega_0\mu_0/k_{z_0}} = \frac{\mu_r/k_z}{1/k_{z_0}} \tag{15a}$$

$$\mu_r = \frac{z\ k_z}{k_{z_0}} \tag{15b}$$

The k_{z_0} in the permeability calculation represents the propagation constant, calculated as the root of the difference of the squares of k_0 and k_c, (16a). The k_c in the permittivity calculation represents the TE_{10} mode wavenumber, calculated as the ratio of π over the metric width of the waveguide, (16b). The k_0 in the permittivity calculation represents the free-space wavenumber, calculated as the ratio of the angular frequency, $\omega = 2\pi f$, over the metric speed of light in free space, (16c).

$$k_{z_0}^2 = k_0^2 - k_c^2 \tag{16a}$$

$$k_c = \frac{\pi}{a} \tag{16b}$$

$$k_0 = \frac{\omega}{c} = \omega\sqrt{\epsilon_0\mu_0} \tag{16c}$$

The complex relative permittivity (17b) is calculated from the wave numbers, (16) and the relative permeability, (15b), to complete material property extraction.

$$k_z^2 = k^2 - k_c^2 \ , \ k_z^2 + k_c^2 = \omega^2 \epsilon_0 \mu_0 \epsilon_r \mu_r \tag{17a}$$

$$\epsilon_r = \frac{k_c^2 + k_z^2}{k_0^2 \ \mu_r} \tag{17b}$$

2.3 Summary

The DCHTWG technique evolved naturally from common field practices with common terms observation. The material characteristics are pulled from the open-form solution using a root search in a NRW algorithm. Three measurements are reduced to two, which are performed at the same time for a reduction in measurement time to one-third.

III. Methodology

Measurements with the dual-chamber high-temperature waveguide (DCHTWG) are an evolution of those with a rectangular waveguide. This is inherent as a process improvement, and this improvement is where the changes lay along with the high-temperature concerns. The design of the DCHTWG takes into consideration the standard size of waveguides that will be attached as a transition to the VNA, alignment holes for scattering-free junctions, axial clamping, and a raised junction interface to handle different thermal expansions. The process is kept simple by using standard hardware external to the DCHTWG. Any advantage in time would be moot with a new process adding to the learning curve.

3.1 Equipment and setup

Quality connections are essential to any EM measurement. Care must be taken to ensure cables are free from tension and excessive bends, RF connectors are correctly torqued, and waveguides are mated without scattering points. Careful calibrations are level with connections in importance. VNA calibrations were completed to the end of a set of standard waveguides prior to data collects. Maintaining the integrity of the calibration in the set-up will keep phase consistency between the multiple measurements and subsequent calculations.

3.1.1 Data Collection.

Baseline tests were accomplished at AFIT using an Agilent Technologies PNA Series two-port vector network analyzer (VNA), model E8362B, using a TRL calibration. High-temperature collects were accomplished at the GE Aviation Cincinnati facility using a Keysight PNA series four-port VNA, model N5222A, using an offset-

short TRL calibration. The collects were accomplished in the X-band using WR-90 sized waveguides and the VNA settings found in Table 1. S-parameter data were saved in a "Citifile Data (Real,imag) *.cti" file format for each temperature and for later processing in MATLAB®. Coaxial cables, of sufficient length to reach the extents of the waveguides, were used to connect the waveguides to the VNA.

Table 1. VNA Test Settings

Parameter	Setting
Frequency	8.2 - 12.4 GHz
IF Bandwith	10 Hz
Stepped	✓
Dwell time	5 msec
System Impedance (Z_0)	1 Ohm

3.1.2 Dual-Chamber High-Temperature Waveguide Hardware.

The DCHTWG was machined from Haynes® 230 [16] to make the two identical 12-inch long pieces. The hardware detailed in this section was initially introduced as a conference presentation [15] during the development of this thesis. The waveguide mating surface was raised to create a lip for the standard waveguide to sit against, while creating a small perimeter gap, shown in Figure 5a. This air gap between the outer perimeters of the standard waveguide and DCHTWG, highlighted in Figure 5b, allows for the different thermal expansion between the dissimilar materials of the waveguides and mounting bolts, while maintaining alignment and preventing spreading, and therefore, scattering sources in the waveguide's RF path.

The externally-mounted springs, at the ends of the tensions rods, are also apparent in Figure 5. High-temperature fatigue of springs and clamps is eliminated by holding the two halves of the DCHTWG in compression with this method. The tension rods are also made of Haynes® 230 to maintain consistent thermal expansion rates. Standard waveguides are secured to the DCHTWG by four threaded bolts after alignment

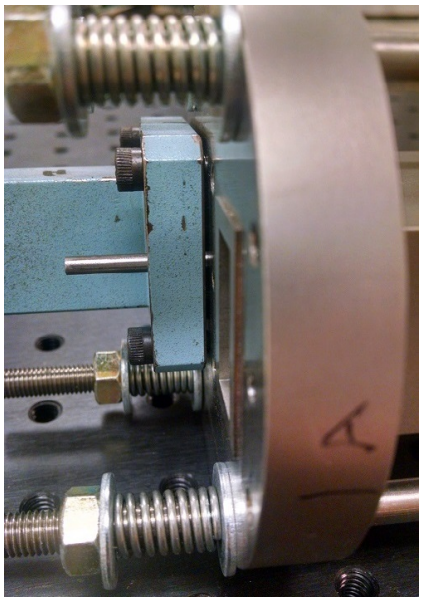

(a) Standard waveguide mounted to DCHTWG with second chamber and lip visible

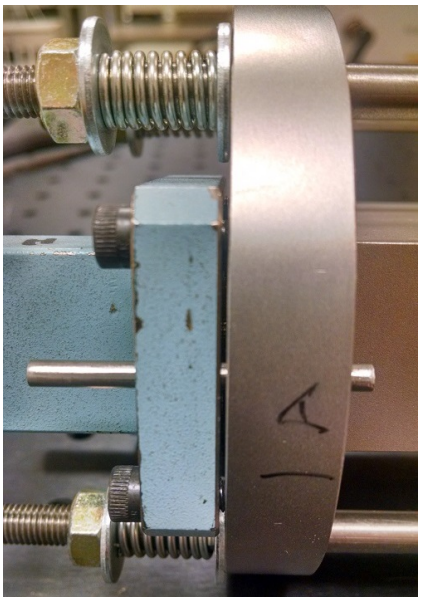

(b) Standard waveguide mounted to DCHTWG with lip gap emphasis.

Figure 5. DCHTWG mounting to a standard waveguide

using precision-machined holes and pins. The precision alignment pins are removed from the center junction of the DCHTWG after they are clamped together and prior to heating to prevent corrosive welding of the two dissimilar metals. Water-cooled waveguide junctions were mounted at the ends of the DCHTWG to isolate the high temperatures needed for the measurement from the rest of the standard hardware.

3.2 Assumptions

The following list enumerates the assumptions of the DCHTWG material characterization method.

1. The material under test is isotropic.
2. The material under test is flat, level, and square.
3. The material fills up the waveguide cross-section fully.

4. The material can withstand the high-temperature environment while maintaining assumptions 2 and 3.
5. The waveguides have a consistent cross-section precision-aligned with each other.
6. The DCHTWG chambers are machined to exact and equivalent lengths.

An isotropic material assumption, 1, is easily accepted with outstanding material manufacturing techniques and by using high-quality research grade materials. Even the most beautiful diamonds will have inclusions, but few random flaws at the microscopic level will not reduce quality sufficiently, as with the materials tested in this research. The same justification can be applied to the quality of the shape of the samples tested, 2 and 3. These qualities allow a straight-forward approach to the math by eliminating any geometric or trigonometric shifts. Any material that would be unsuited for the high-temperature environment and especially those that would change shape significantly enough, 4, are better measured through free-space or other measurement methods.

High-quality precision measurement equipment is a requirement for accurate results. All standard waveguide equipment used for this thesis are research quality; allowing for scattering-free connections, 5. The experimental DCHTWG was produced through electrical discharge machining to exacting dimensions, 6. The equivalence between the two chambers was checked through measurement of both chambers and a phase differential calculation, Figure 6.

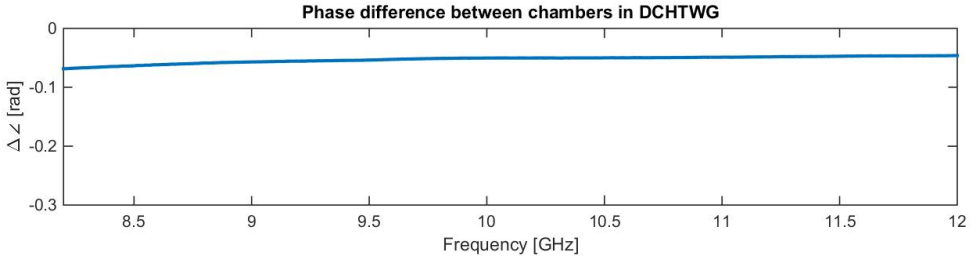

Figure 6. DCHTWG chamber check

3.3 Baseline Development

Initial runs were accomplished using the standard NRW technique at room temperature to determine baselines and develop MATLAB® analysis code, found in Appendix B. This set-up is shown in Figure 7. Four runs were collected for each condition to

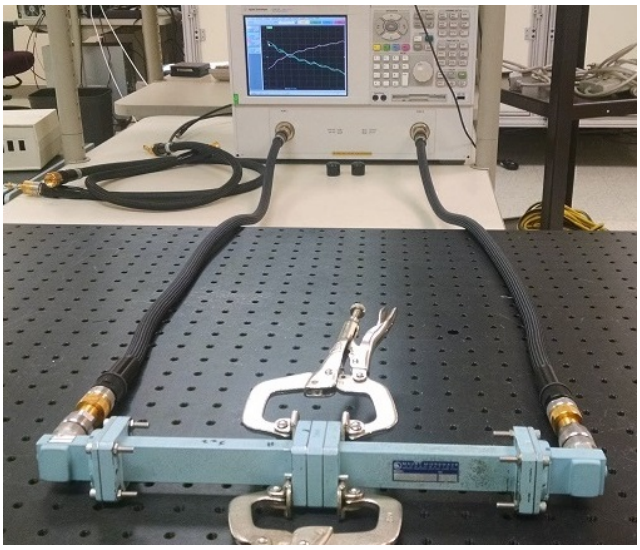

Figure 7. NRW technique experimental set-up

observe repeatability uncertainty, and combined with the uncertainty analysis applied from subsection 4.1.1. These calibration runs were accomplished using samples of mica, FGM-125 [17] microwave-absorbent material (MAGRAM), and a polymer sample made through additive manufacturing. These materials were chosen due to their varied dielectric properties and ready availability. First look at the mica sample is shown in Figure 8 and the MAGRAM sample is shown in Figure 9.

The DCHTWG was then installed in-line to conduct verification collects of the hardware, as seen in Figure 10. These runs were accomplished with the 2-port VNA collecting the sample-loaded data, then reattached to the second chamber to collect the empty data required for the calculations. The DCHTWG look at the mica sample is shown in Figure 11, and the MAGRAM sample is shown in Figure 12.

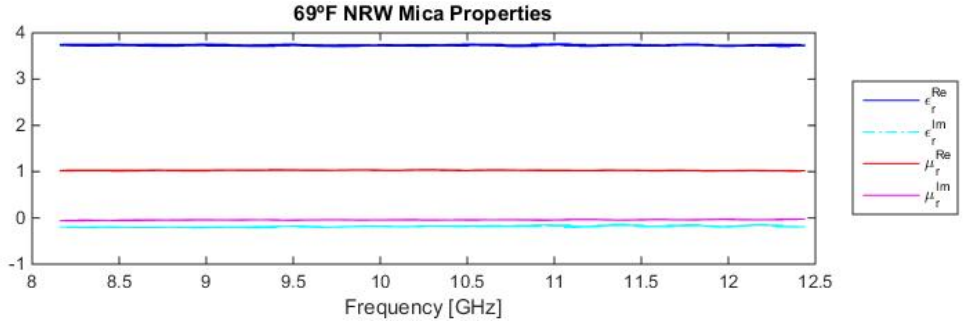

Figure 8. Mica analysis using NRW

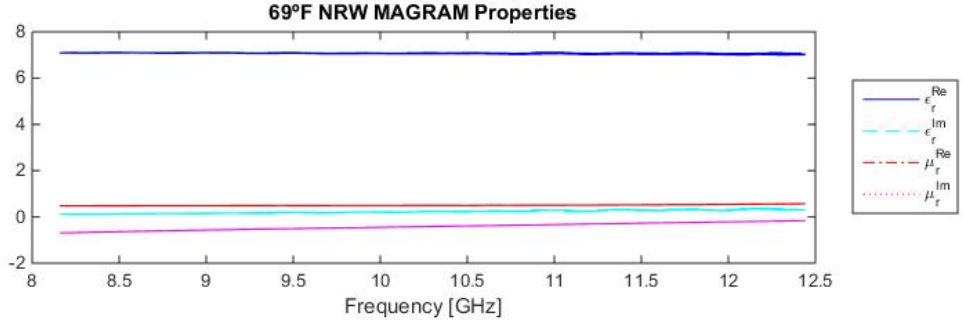

Figure 9. MAGRAM analysis using NRW

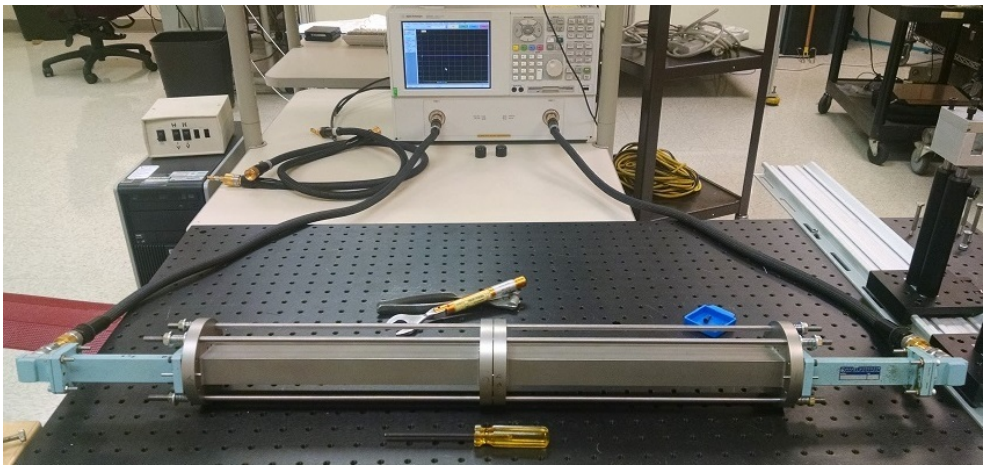

Figure 10. DCHTWG technique developmental set-up

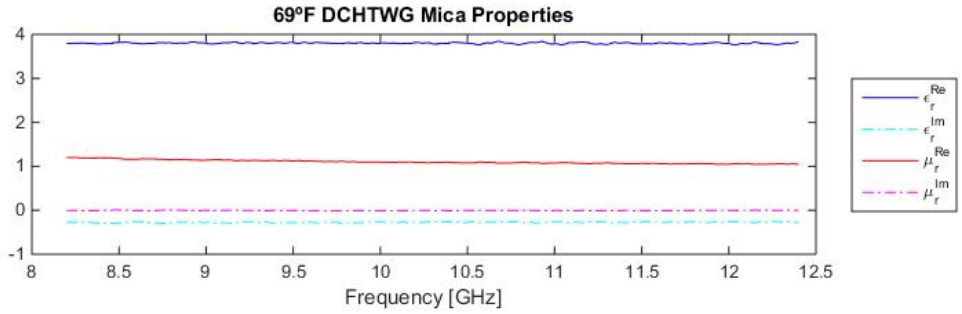

Figure 11. Mica analysis using DCHTWG

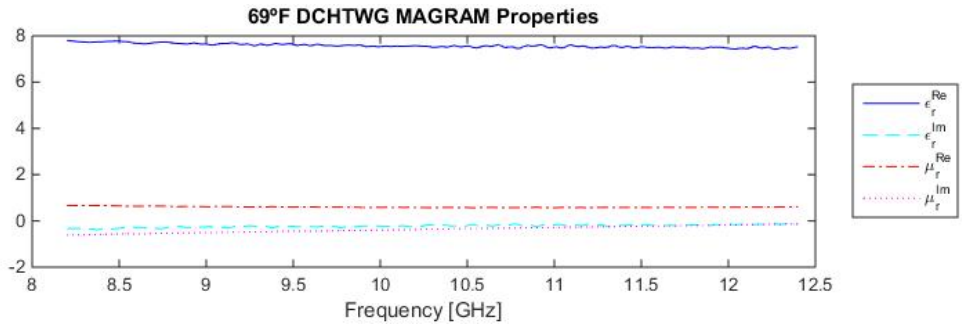

Figure 12. MAGRAM analysis using DCHTWG

Looking at the difference between the two measurements shows a strong correlation, in Figure 13 for the mica sample and Figure 14 for the MAGRAM sample. The comparison was done with a difference over mean calculation. The positive results shown in these charts provide the confidence to move on to high-temperature measurements.

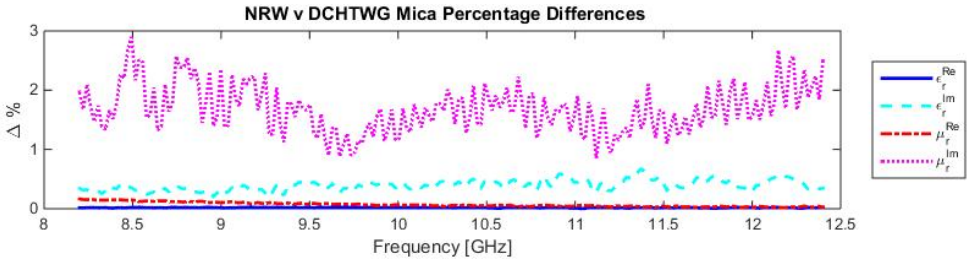

Figure 13. NRW v DCHTWG percentage difference for Mica

Configuration control runs were also accomplished by matching the different ports

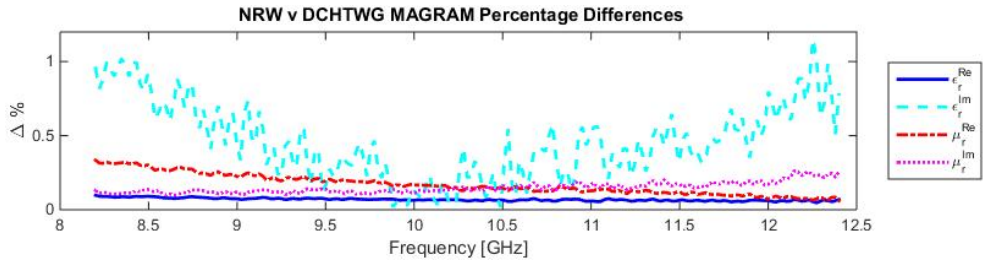

Figure 14. NRW v DCHTWG percentage difference for MAGRAM

of the DCHTWG in the multiple permutations. This was accomplished to check for consistent measurements and to refine the data collecting process. This highlighted the necessity of ensuring a flush mount of the standard waveguide to the relatively narrow lip of the DCHTWG. The data collected checking the configuration control showed no discernible differences, providing further confidence in the hardware for continuing to high-temperature collects.

3.4 High-Temperature Runs

High-temperature runs were accomplished using samples of alumina (Al_2O_3) [18]. Additional samples were pursued, but unavailable for testing with time and classification restrictions. Alumina was selected due to its ready availability and well known properties for initial proof of concept. The samples were loaded into the DCHTWG, as shown in Figure 15. The sample loaded DCHTWG was then placed

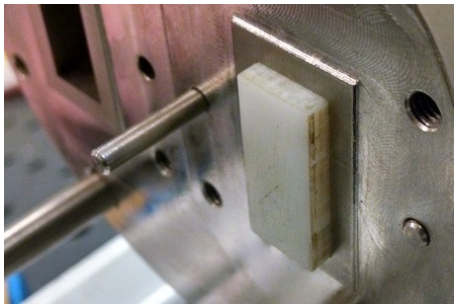

Figure 15. DCHTWG with material partially loaded (not flush) into one chamber

in a clam-shell style oven for the heating, as shown in Figure 16. Additional pieces of

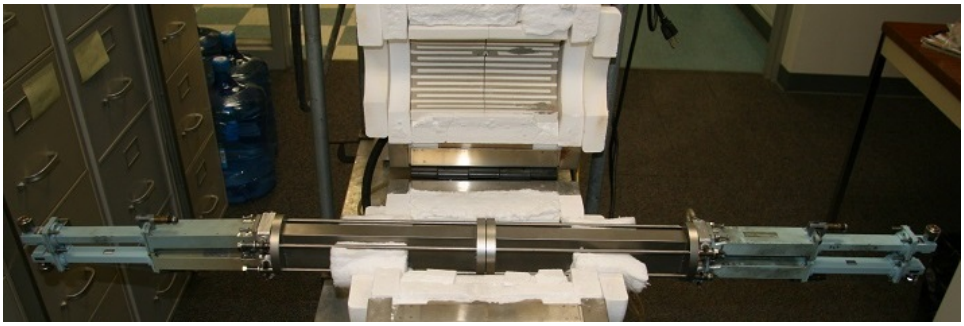

Figure 16. DCHTWG in clam-shell oven prior to heating

high-temperature insulation were placed around the hardware at the ends of the oven, as seen in Figure 17, to keep the high temperatures of the oven in and gaining heating efficiency. Keeping the heat in is also required to isolate the sensitive measurement hardware of the cables and VNA.

Figure 17. Close-up of DCHTWG in clam-shell oven prior to heating

The materials were incrementally heated to the temperatures shown in Table 2. The test temperatures were chosen to see any noticeable trends in the material performance based on the temperature. Temperatures were measured with a thermocouple placed as close to the sample as possible. Temperatures were allowed to stabilize during the heating process to ensure a steady state during the measurement window of approximately 36 seconds.

Table 2. DCHTWG Test Matrix

Temperature	Material
72F	Alumina
250F	Alumina
500F	Alumina
750F	Alumina
1000F	Alumina

3.5 Summary

The DCHTWG measurement methodology is shown as an expansion of standard measurement techniques. The heating of the material in the DCHTWG uses the same method as standard high-temperature rectangular waveguide measurements. The advantage of the method is in the concurrent collection of sample-loaded and empty waveguides, which are in the same heated environment.

IV. Results and Analysis

EM material characterization is accomplished using a dual-chamber high-temperature waveguide (DCHTWG) and a position independent analysis. A Baker-Jarvis [4] uncertainty analysis is performed on the collected data. Process improvements are observed with change recommendations.

4.1 Results

The S-parameter data collected from the VNA is processed in MATLAB®, using the code available in Appendix A, to extract the complex permittivity and permeability of the measured material.

4.1.1 Uncertainty Analysis.

Uncertainty analysis was conducted using the Baker-Jarvis [4] calculation technique. The independent sources of uncertainty from Baker-Jarvis, Vanzura, and Kissick are listed below.

1. S-parameter measurement
2. Sample perimeter gaps
3. Sample length
4. Connections
5. Reference plane
6. Mode order

These uncertainties are the results of many factors. The S-parameter measurement uncertainties, 1., are systematic and caused by signal directivity and crosstalk, source and load mismatches, and reflection and transmission tracking [19] in the VNA. The sample perimeter gaps, 2., are a systematic uncertainty due to the differing high temperature material thermal expansions. The sample length, 3., is a random uncertainty from measurement uncertainty from the caliper measurement and thermal

expansion. The connections, 4., create a systematic and random uncertainty due to alignment and cable movement. The reference plane, 5., drives a random uncertainty caused by any transposition of the material in the waveguide. The mode order, 6., is another systematic uncertainty from unintended modes being excited or destructively interfered from sample thickness errors.

Some of these uncertainties can be minimized or accepted. Item 6 can be accepted with material thickness being less than a quarter wavelength at the highest frequency. The position independence inherent with the DCHTWG technique eliminates any uncertainty from Item 5 and minimizes those from Item 2 [13] to an acceptable level. Uncertainty source 4 is minimized with precision alignment pins and quality calibrations to eliminate unwanted scattering surfaces. The sample length uncertainty source, 3, is unavoidable and the most significant uncertainty source. The sample length uncertainty is calculated from measurement uncertainty, observed in Figure 18 and broadened with summing the thermal expansion of the sample. S-parameter

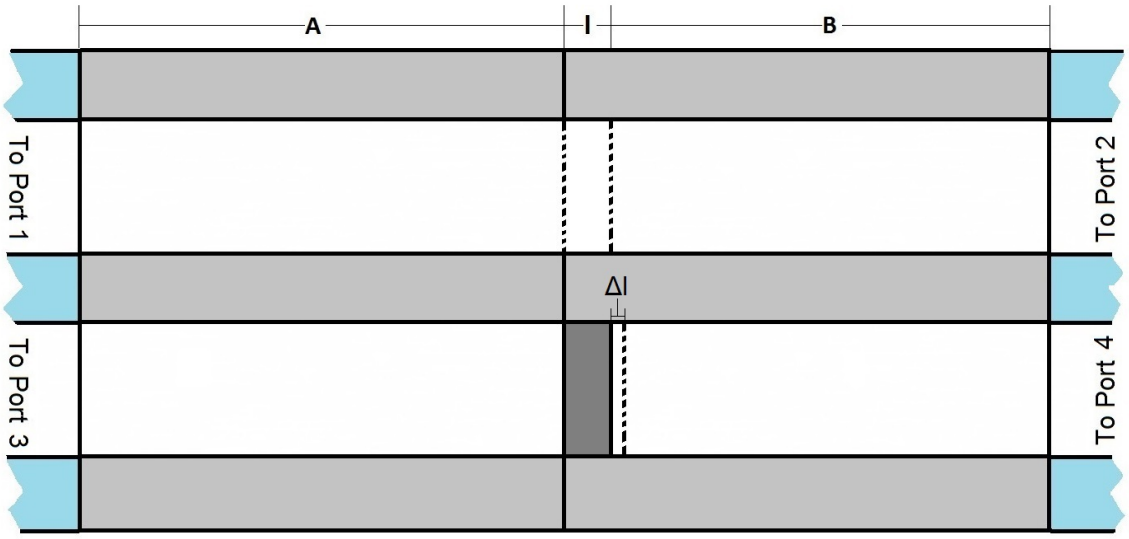

Figure 18. Sample-loaded DCHTWG sample depth uncertainty

uncertainty, 1, could not be analyzed as further research is needed to see the interplay

of the multiplication from the averaging.

The sample length uncertainty in (18a), $\Delta\ell$, comes from uncertainty in the measurement, $\Delta\ell_0$, and the thermal expansion, $\delta\ell$. The sum of the absolute values are used to analyze the worst case scenario. The thermal expansion is the product of the coefficient of thermal expansion, α; the change in temperature, ΔT; and the initial length of the material, ℓ [20].

$$\Delta\ell = |\Delta\ell_0| + |\delta\ell| \tag{18a}$$

$$\delta\ell = \alpha(\Delta T)\ell \tag{18b}$$

The standard deviations of the material parameters are shown in the four relations in (19), with the single prime denoting the real component and the double prime as the imaginary.

$$\sigma_{\epsilon'} = \sqrt{\left(\frac{\partial\epsilon'}{\partial\ell}\right)^2\sigma_\ell^2},\ \sigma_{\epsilon''} = \sqrt{\left(\frac{\partial\epsilon''}{\partial\ell}\right)^2\sigma_\ell^2} \tag{19a}$$

$$\sigma_{\mu'} = \sqrt{\left(\frac{\partial\mu'}{\partial\ell}\right)^2\sigma_\ell^2},\ \sigma_{\mu''} = \sqrt{\left(\frac{\partial\mu''}{\partial\ell}\right)^2\sigma_\ell^2} \tag{19b}$$

First the standard deviation of the length must be determined through (20).

$$\sigma_\ell = \sqrt{var[\ell]} = \sqrt{E[\ell^2] - E[\ell]^2} \tag{20}$$

The expected value function, $E[\ ]$, is defined in (21a) and calculated in (21c) and (21d), with the probability function of the discrete uniform distribution posed by the

length measurements in (21b).

$$E[x] = \sum_{k-1}^{K} x_k P(x_k) = \int_{-\infty}^{\infty} xP(x)dx \tag{21a}$$

$$P(\ell) = \frac{1}{2\Delta\ell} \tag{21b}$$

$$E[\ell^2] = \int_{\ell_0-\Delta\ell}^{\ell_0+\Delta\ell} \frac{\ell^2}{2\Delta\ell} d\ell = \frac{\ell^3}{3 \cdot 2\Delta\ell}\Big|_{\ell_0-\Delta\ell}^{\ell_0+\Delta\ell} = \ell_0^2 + \frac{\Delta\ell^2}{3} \tag{21c}$$

$$E[\ell]^2 = \left[\int_{\ell_0-\Delta\ell}^{\ell_0+\Delta\ell} \frac{\ell}{2\Delta\ell} dx\right]^2 = \left[\frac{\ell^2}{2 \cdot 2\Delta\ell}\Big|_{\ell_0-\Delta\ell}^{\ell_0+\Delta\ell}\right]^2 = \ell_0^2 \tag{21d}$$

Working the solutions from (21c) and (21d) back into (20) results in a simple form for the standard deviation of the depth of the material shown in (22).

$$\sigma_\ell = \sqrt{\ell_0^2 + \frac{\Delta\ell^2}{3} - \ell_0^2} = \frac{\Delta\ell}{\sqrt{3}} \tag{22}$$

The partial derivative of the parameter with respect to the length can be represented numerically for the case of the real permittivity in (23).

$$\frac{\partial\epsilon'}{\partial\ell} = \frac{\epsilon'(\ell_0 + \Delta\ell) - \epsilon'(\ell_0)}{\Delta\ell} \tag{23}$$

When combining the results from (22) and (23) back into (19) a simple solution for each material parameter's standard deviation is resolved in (24), which can be solved analytically in MATLAB®. The magnitude is used to pick the positive value

from the root of the square, originally from (19).

$$\sigma_{\epsilon'} = \left|\epsilon'(\ell_0 + \Delta\ell) - \epsilon'(\ell_0)\right| / \sqrt{3} \tag{24a}$$

$$\sigma_{\epsilon''} = \left|\epsilon''(\ell_0 + \Delta\ell) - \epsilon''(\ell_0)\right| / \sqrt{3} \tag{24b}$$

$$\sigma_{\mu'} = \left|\mu'(\ell_0 + \Delta\ell) - \mu'(\ell_0)\right| / \sqrt{3} \tag{24c}$$

$$\sigma_{\mu''} = \left|\mu''(\ell_0 + \Delta\ell) - \mu''(\ell_0)\right| / \sqrt{3} \tag{24d}$$

The error bars used for the material parameters in the following sub-section use these doubled calculated standard deviations from (24).

4.1.2 Data Analysis.

The high-temperature runs were accomplished with a sample of alumina [18]. Tests were performed at the temperatures from Table 2. Starting at room temperate, measured at 72°F, the alumina sample was calculated to have a frequency variant real permittivity between 10.5 and 11.5 and a real permeability around 1 with imaginary values for both about 0, as seen in Figure 19. These values are consistent with known

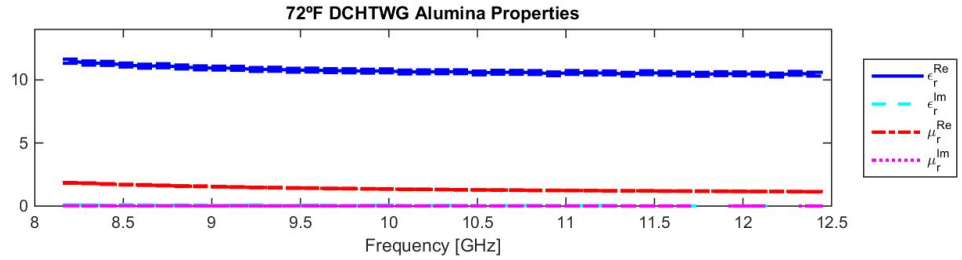

Figure 19. Alumina room temperature DCHTWG analysis

values for the non-magnetic ceramic across the frequency range measured, including the downward trend of the real parts with increasing frequency shown here. The high-temperature runs were continued at 250°F, Figure 20a, at 500°F, Figure 20b, at 750°F, Figure 20c, and at 1000°F, Figure 20d. The results at all temperatures show

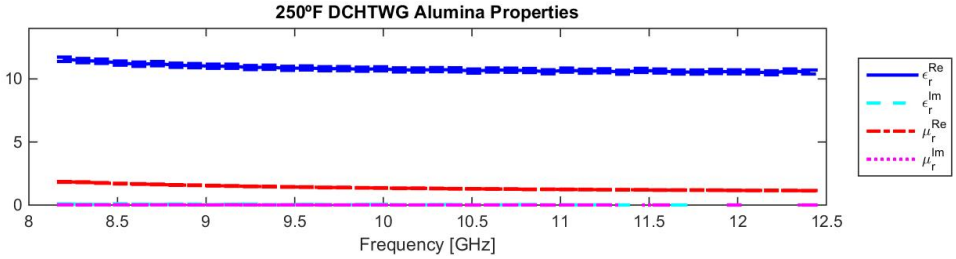

(a) Alumina 250°F analysis using DCHTWG

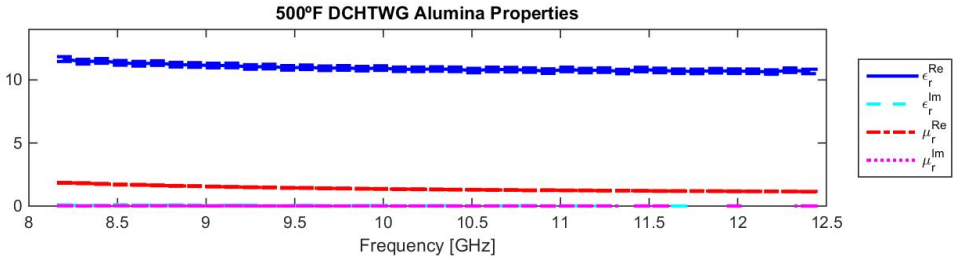

(b) Alumina 500°F analysis using DCHTWG

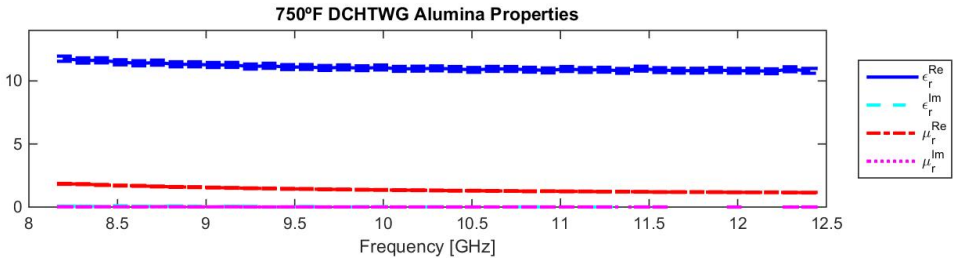

(c) Alumina 750°F analysis using DCHTWG

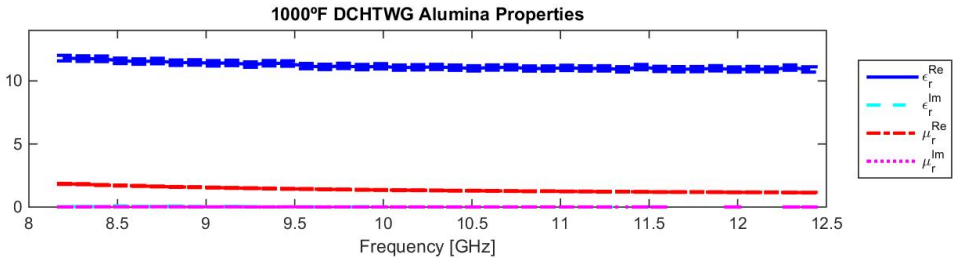

(d) Alumina 1000°F analysis using DCHTWG

Figure 20. Alumina high-temperature analyses using DCHTWG

a consistent smooth frequency trend and a lossless response.

Comparing the room-temperature measurement to the highest temperature collect shows, in Figure 21, the expected rise in the permittivity of the sample with temperature, while the permeabilities remain consistent around 1.

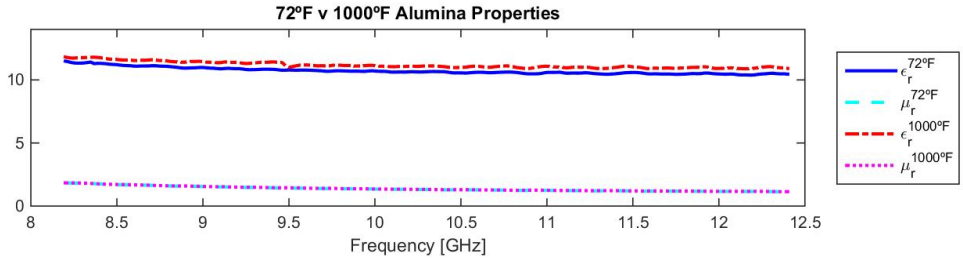

Figure 21. Alumina room-temperature v 1000°F DCHTWG analysis

4.2 Lesson Learned

As an initial exploration into this theory, there were observations on the process. These observations led to process and system improvements that were implemented as applicable. Hardware improvements were noted, but not implemented due to the ability to continue research as constructed and schedule/cost risk.

4.2.1 Set-Up.

Special attention and handling was noted during set-up of the system and baseline tests. The most imperative observation is the quality of the calibration. A lack of attention paid to cable shifting and waveguide mating surfaces during the calibration procedure had and will lead to unacceptable data shifts. The flush and precision aligned waveguide mating proved to be an area of concern during the calibration and measurements. The raised interface on the DCHTWG required careful torquing of the mounting bolts, when mating standard waveguides, to ensure flush mounting. The

system's combined length and weight necessitated judicious use of precision alignment pins and support to keep the system free of unwanted scattering sources.

Erroneous data was collected during initial high-temperature tests. After deeper analysis, it was determined to be due to additional waveguide lengths inserted between the tier 1 calibration plane and the DCHTWG. These additional waveguides were inserted as part of the heat sink to isolate the high-temperature from the oven away from the waveguide RF launchers and coaxial cables. The inconsistency in lengths of these additions between the two chambers induced an uncharacterized phase shift that prevented a proper resolution, as seen in Figure 22.

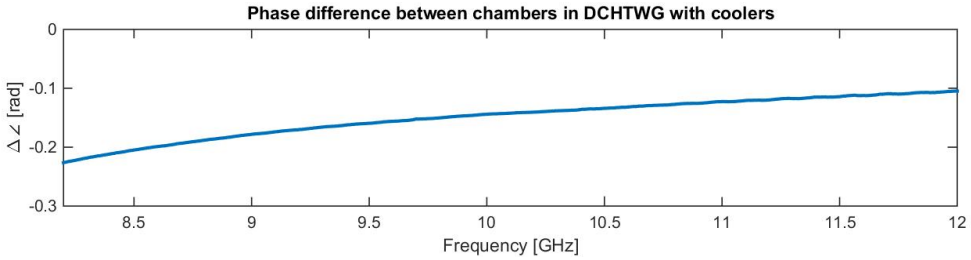

Figure 22. DCHTWG with cooling adapters chamber check

4.2.2 DCHTWG Hardware.

Enhancements to the hardware became apparent during set-up of the hardware for high-temperature collects. These enhancements will increase ease of set-up and accurate alignment. Proper planning of accessory location is required for spatial deconfliction with the increased amount of accessories necessary for high-temperature testing; like the tension rods, mounting bolts, coolant lines, precision alignment pins/holes, and temperature probe points. The crowded real estate is demonstrated in Figure 23.

A special case of orientation was found with the construction of the DCHTWG used for this testing. The orientation of the waveguide chambers are aligned in an

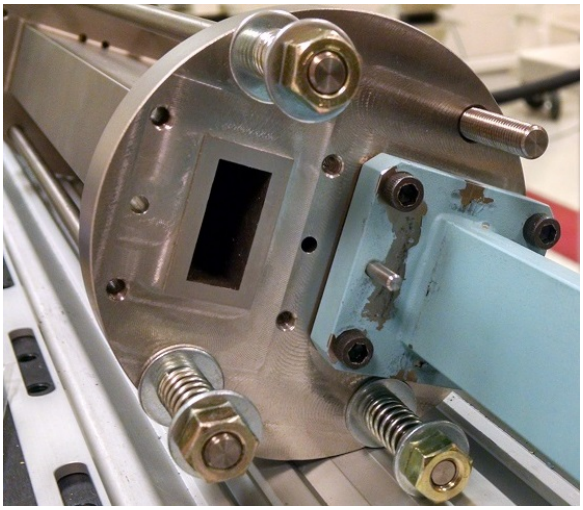

Figure 23. DCHTWG mounting face

over-under (O/U) arrangement with the wide axes being next to each other. This O/U orientation led to the RF launchers and coaxial cables being oriented π radians from each other, as shown in Figure 24. The opposing directions let one cable hang

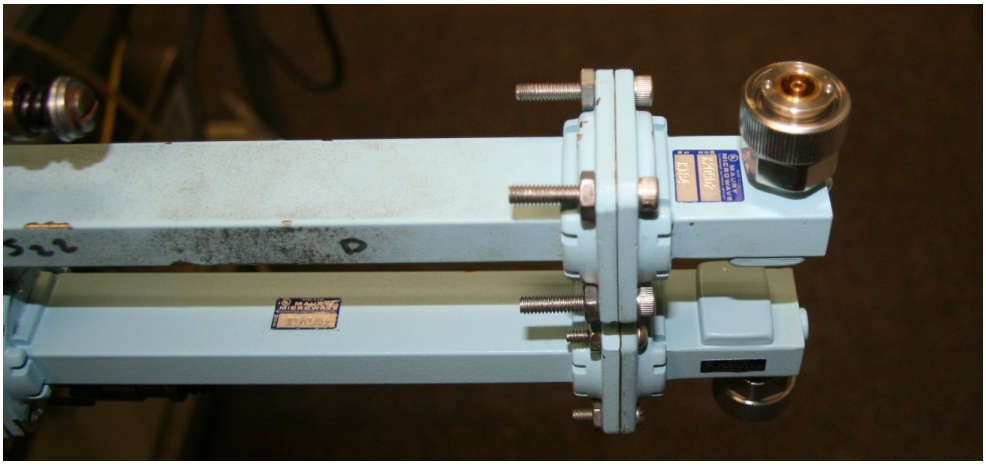

Figure 24. Coaxial-Rectangular waveguide adapters

and the other stick up, creating differing tensions and an unnecessary $\frac{\pi}{2}$ bend. A side-by-side (SxS) orientation, with the narrow axes being next to each other, benefits in sending the cables and launchers in the same direction, allowing consistent tension and less bends in the cabling. An additional benefit of the SxS orientation is increased

surface area over the chambers, which provides more evenly dispersed heating, which in turn could decrease heating times.

Standard precision alignment pins and holes are likely to oxidize and seize in the high-temperature environment. Larger precision alignment holes and pins made of the same resistant alloy as the waveguide reduce the risks while still enabling precision alignment through the heating. Expanding the raised mounting area for a wider footprint will avoid torsion from poor torquing to keep the precision alignment true during mounting of the standard waveguides. A final modification is to mill flat faces on the outer perimeter of the mounting flange, rather than the round cut, to stabilize the system for bench-top analysis.

Issues with the multiple hardware junctions led to minimizing as many connections as possible. The inclusion of the heat sink waveguide adapter put coolant lines cluttering the mounting area, an additional two waveguide connections, and a probable length delta between the two chambers. Future DCHTWGs could have a cooling jacket manufactured into the apparatus to relocate the lines more efficiently while reducing excess waveguide junctions. This combination then makes the DCHTWG a one-stop piece of hardware to start rapid and simple high-temperature material measurements.

The next version of the DCHTWG is shown in Figure 25, resolving the issues discussed in this section. The SxS orientation opens space for an integral coolant passage going across the top of the chamber's long edges. Two high temperature precision alignment pin locations are locate near the central axis of the waveguide. Flats are placed at the top, bottom, and both side edges to prevent rotation during hardware mounting. Finally, all low-temperature fixtures and the tension rod capability remain.

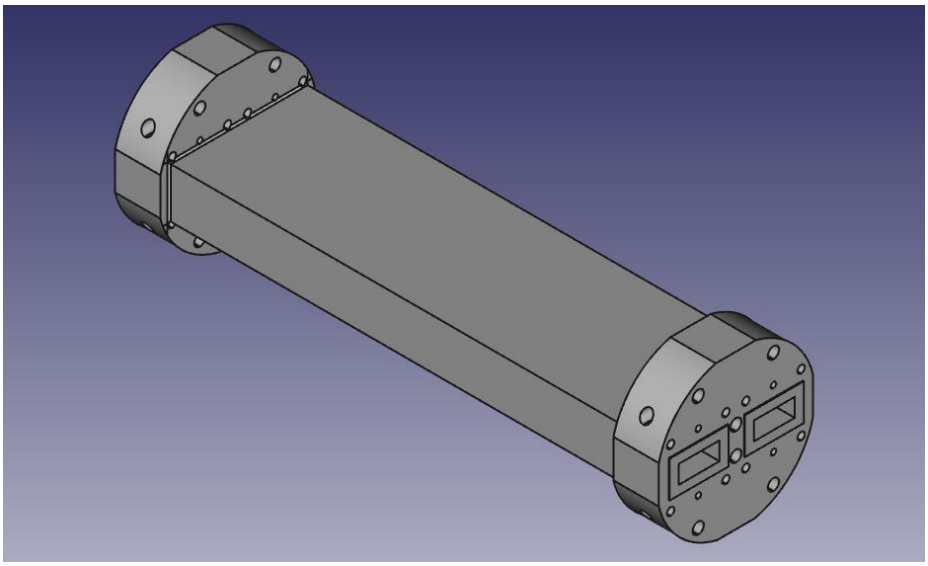

Figure 25. Proposed DCHTWG evolutionary design

4.3 Summary

Data collected using the DCHTWG was analyzed using the theory presented in Ch. II and the methodology detailed in Ch. III. The results presented in this chapter demonstrate the effectiveness of the DCHTWG compared to current industry standards. The uncertainty analysis demonstrates the quality of the system.

V. Conclusion

5.1 Research Effectiveness

The DCHTWG is presented as a new technique for high-temperature EM isotropic material characterization. The position independent approach developed in this thesis enables single-run measurements of isotropic materials at high temperatures, compared to the standard three-run measurement set. This wavelength scalable method allows for rapid, one-third time, high-temperature material characterization. It is shown that material properties are within a few percentage points of standard NRW methods. The DCHTWG technique does not sacrifice significant precision in order to return the gains in collection time.

The process and hardware vetted through this thesis demonstrate promising results. United States Air Force research labs and industry partners are ready to take this theory and the evolved hardware design to regular practice in the development and research of materials with national security applications. The effective reduction in measurement time and effort will help the otherwise lengthy acquisition process of advanced materials.

5.2 Future Research

The lessons discussed involving test set-up, in section 4.2.1, can and were implemented immediately to high-temperature material measurement. Research into length differentials between waveguides and their effects on the perceived phase at the calibration plane can provide correction terms when adding uncalibrated cooling adapters. Additional hardware evolutionary changes can be examined to optimize the design; such as relative placement between the chambers, high-temperature precision alignment pins, coolant passages, and tension rods.

In addition to the hardware lessons learned discussed in section 4.2.2, the current hardware can be utilized for further research. This research merely scratched the surface of available materials in order to prove the validity of the theory. The effectiveness of this process can be researched on different materials, including anisotropic materials to observe relative effects. With the plethora of materials available to design engineers, this hardware and theory can be applied to improve the performance of many systems with defense, aerospace, communications, or any other system with RF applications at elevated temperatures.

Appendix A.

```
%% Network Analyzer data processing, DCHTWG process, Capt Jeff Sovern
% Thesis code
clc,  clear, close all
LFS = 10;       % legend font size
mtd = 'DCHTWG';
%% VNA port quantity check
vna = input('Four-port or two-port network analyzer used for ...
    collection? (4 or 2) ');
%% Load data
            if vna == 2
     %% Load the empty guide data file
   disp('   Select empty guide file... ')
[emptyfilename, pathname] = uigetfile( ...
{'*.cti;*.xls;*.txt;*.s2p','Network Analyzer Data';...
   '*.m',  'Code files (*.m)'; ...
   '*.mat','MAT-files (*.mat)'; ...
   '*.xls','Excel files (*.xls)'; ...
   '*.*',  'All Files (*.*)'}, ...
   'Pick a file');
if isequal(emptyfilename,0)
   disp('User selected Cancel')
else
disp(['User selected empty guide file: ...
    ',fullfile(pathname,emptyfilename)])
   [pn,file,extensione] = fileparts(emptyfilename);
end
    %% Load the empty guide network analyzer data
if isequal(extensione,'.cti')
    [freqe,s11me,s12me,s21me,s22me] = cti_data_load2(emptyfilename);
```

```
elseif isequal(extensione,'.s2p')
    [freqe,s11me,s12me,s21me,s22me] = s2p_data_load(emptyfilename);
elseif isequal(extensione,'.xls')
    [freqe,s11me,s12me,s21me,s22me] = xls_data_load(emptyfilename);
end
    %% Load the filled guide data file
   disp('   Select material loaded guide file... ')
[samplefilename, pathname] = uigetfile( ...
{'*.cti;*.xls;*.txt;*.s2p','Network Analyzer Data';...
   '*.xls','Excel files (*.xls)'; ...
   '*.m',  'Code files (*.m)'; ...
   '*.mat','MAT-files (*.mat)'; ...
   '*.*',  'All Files (*.*)'}, ...
   'Pick a file');
if isequal(samplefilename,0)
   disp('User selected Cancel')
else
   disp(['User selected material data file: ', fullfile(pathname, ...
      samplefilename)])
   [pn,file,extensions] = fileparts(samplefilename);
end
    %% Load the filled guide network analyzer calibration data
if isequal(extensions,'.cti')
    [freqs,s11ms,s12ms,s21ms,s22ms] = cti_data_load2(samplefilename);
elseif isequal(extensions,'.s2p')
    [freqs,s11ms,s12ms,s21ms,s22ms] = s2p_data_load(samplefilename);
elseif isequal(extensions,'.xls')
    [freqs,s11ms,s12ms,s21ms,s22ms] = xls_data_load(samplefilename);
end
    %% consolidate to one frequency value
    if isequal(freqe,freqs)
        freq = freqe;   % Frequency [Hz]
```

```
59      end
60          clear freqe freqs;   % reducing variables hogging up memory
61  elseif vna == 4;
62      %% Load the 4-port guide data file
63     disp('   Select 4-port guide file... ')
64  [fourportfilename, pathname] = uigetfile( ...
65  {'*.cti;*.xls;*.txt;*.s2p','Network Analyzer Data';...
66     '*.xls','Excel files (*.xls)'; ...
67     '*.m',  'Code files (*.m)'; ...
68     '*.mat','MAT-files (*.mat)'; ...
69     '*.*',  'All Files (*.*)'}, ...
70     'Pick a file');
71  if isequal(fourportfilename,0)
72     disp('User selected Cancel')
73  else
74     disp(['User selected material data file: ...
           ',fullfile(pathname,fourportfilename)])
75     [pn,file,extensions] = fileparts(fourportfilename);
76  end
77  %% Material chamber location check
78  % Check if the material is in the top (1-2) or bottom (3-4) chamber
79      port = input('Which chamber is the material mounted? (12 or 34) ');
80  if port == 12;
81          % Load the backwards 4-port guide data
82  [freq,s11me,s21me,s12me,s22me,s11ms,s21ms,s12ms,s22ms] = ...
       cti_data_load4b(fourportfilename);
83      fprintf('\t Unexpected chamber, but I got your back! \n')
84  elseif port == 34;
85          % Load the 4-port guide data
86  [freq,s11me,s21me,s12me,s22me,s11ms,s21ms,s12ms,s22ms] = ...
       cti_data_load4(fourportfilename);
87      fprintf('\t Expected chamber, Good Job!\n')
```

```
end
%% GHz frequency
    freqG = freq/1e9;        % for plot scaling [GHz]
                end

%% Material Port location check
% This mistake was made more than once, so here is a check and
% correction if the material is erroneously placed on the port 1
% side of the waveguide junction
% ==========|==========       ==========|==========
%        matl|                          |matl
% port 1 matl|    port 2        port 1   |matl port 2
%        matl|                          |matl
% ==========|==========       ==========|==========
    port = input('Which port side is the material mounted? (1 or 2) ');
if port == 1;
% If you have the material in the port 1 side instead of the port 2, use
% the following to swap the paramaters for the expectations of the
% following calculations
    s11msnew = s22ms;
    s22msnew = s11ms;
    s11ms = s11msnew;
    s22ms = s22msnew;
        clear s11msnew s22msnew; % reducing variables hogging up memory
    fprintf('\t Wrong side, but I got your back! \n')
elseif port == 2;
    fprintf('\t Good Job!\n')
end
%%  Input the material data
tempF = input('What is the temperature of the collection? ( F ) ');
matl = input('What material is loaded in the waveguide? (if nothing ...
    type air) ','s');
```

```
% Alumina sample: 1.957mm
% Alumina sample 2: 0.076" = 1.93mm   0.0254
% Mica Sample material Thickness: 3.23mm0.01
% Magram FGM125 Sample material Thickness: 3.17mm0.02
% White Sample material Thickness: 4.13mm
% insert length: 152.50 mm
d = 1e-3 * input('What is the material thickness? [mm] ');
 delta_d = 1e-3 * input('     What is the material thickness variance? ...
    [mm] ');
%%  Input the waveguide data
a = 22.86e-3;    b = 10.16e-3; % wr-90 x-band, 0.9" x 0.4" [mm]
eps0 = 8.854187817e-12; % vacuum permittivity [F/m]
mu0 = pi * 4e-7;        % vacuum permeability [F/m]
c = 299792458;          % light speed [m/s]
omega = 2*pi .* freq;   % angular frequency [rad/s]
k0 = omega ./ c;        % freespace wavenumber
kc = pi/a;              % TE10 mode
kz0 = sqrt(k0 .^2 - kc .^2);
%% show the raw data
        theta1 = unwrap(angle(s11ms));   % unwrap corrects phase jump
        theta2 = unwrap(angle(s21ms));   % unwrap corrects phase jump
        theta3 = unwrap(angle(s12ms));   % unwrap corrects phase jump
        theta4 = unwrap(angle(s22ms));   % unwrap corrects phase jump
figure(1);
    set(gcf,'units','normalized','position',[0 0 1 1]) % full screen fig
subplot(2,2,1)
    plot(freqG,real(s11ms),'b-', ...
          freqG,real(s21ms),'m-', ...
           freqG,real(s12ms),'y--', ...
            freqG,real(s22ms),'c--')
    xlabel('Frequency [GHz]'),     ylabel('S-Parameter')
    title(['' num2str(tempF) ' F  DCHTWG Raw S-Parameters, Complex ...
```

```
        Real'])
150     axis square
151     legend('s_{11}^{Re}','s_{21}^{Re}','s_{12}^{Re}','s_{22}^{Re}',...
152                 'Location','eastoutside','FontSize',LFS)
153 subplot(2,2,2)
154     plot(freqG,abs(s11ms),'b-',...
155           freqG,abs(s21ms),'m-',...
156            freqG,abs(s12ms),'y--',...
157             freqG,abs(s22ms),'c--')
158     xlabel('Frequency [GHz]'),     ylabel('S-Parameter, Magnitude')
159     title(['' num2str(tempF) ' F  DCHTWG Raw S-Parameters, Magnitude'])
160     axis square
161     legend('|s_{11}|','|s_{21}|','|s_{12}|','|s_{22}|',...
162                 'Location','eastoutside','FontSize',LFS)
163 subplot(2,2,3)
164     plot(freqG,imag(s11ms),'b-.',...
165           freqG,imag(s21ms),'m-.',...
166            freqG,imag(s12ms),'y--.',...
167             freqG,imag(s22ms),'c--.')
168  xlabel('Frequency [GHz]'),     ylabel('S-Parameter')
169  title(['' num2str(tempF) ' F  DCHTWG Raw S-Parameters, Complex ...
        Imaginary'])
170  axis square
171  legend('s_{11}^{Im}','s_{21}^{Im}','s_{12}^{Im}','s_{22}^{Im}',...
172               'Location','eastoutside','FontSize',LFS)
173 subplot(2,2,4)
174     plot(freqG,theta1/pi,'b-',...
175           freqG,theta2/pi,'m-',...
176            freqG,theta3/pi,'y--',...
177             freqG,theta4/pi,'c--')
178  xlabel('Frequency [GHz]'),     ylabel('S-Parameter, Angle')
179  title(['' num2str(tempF) ' F  DCHTWG Raw S-Parameters, Angle'])
```

```
180  axis square
181  legend('\angle s_{11}','\angle s_{21}','\angle s_{12}','\angle ...
       s_{22}',...
182                 'Location','eastoutside','FontSize',LFS)
183 %% De-embed Technique #3 (additional waveguide, empty measurement)
184 %  s11 = -sqrt( (s11ms .*s22ms .*exp(-j *kz0 *d *2)) ./(s21me ...
      .*s12me) );
185 %  s21 = sqrt( (s21ms .*s12ms .*exp(-j *kz0 *d *2)) ./(s21me ...
      .*s12me) );
186 %      check = -sign(angle(s21));
187 %  s21 = check .* s21;
188
189 % split s11 (into s11n & s22n) & s21 to normalized versions & do ...
      angle test
190     s11n = s11ms ./s21me;
191 %         t1 = unwrap( atan2(imag(s11n),real(s11n)),1 );
192 %         t1 = atan2( imag(s11n),real(s11n) ); % different ways to ...
      skin cat
193         t1 = unwrap(angle(s11n));   % unwrap corrects for phase jump
194     s22n = (s22ms .* exp(-1i *kz0 *d *2) ) ./s12me;
195         t2 = unwrap(angle(s22n));   % angle finds complex pair phase ...
              angle
196     s21n = (s21ms .* exp(-1i *kz0 *d)) ./s21me;
197         t3 = unwrap(angle(s21n));
198     s12n = (s12ms .* exp(-1i *kz0 *d)) ./s12me;
199         t4 = unwrap(angle(s12n));
200 s11 = sqrt( abs(s11n) .* abs(s22n)) .*exp(1i * (t1 + t2)/2);
201 s21 = sqrt( abs(s21n) .* abs(s12n)) .*exp(1i * (t3 + t4)/2);
202 %% Branch cut test
203 t1 = unwrap( angle(s11n) );
204 t2 = unwrap( angle(s21n) );
205 t3 = unwrap( angle(s12n) );
```

```
206 t4 = unwrap( angle(s22n) );
207 if t1 > (pi/2) & t2 < (-pi/2) %#ok<*AND2>
208     s11 = -1 .*s11;
209     branchcase1 = 1;
210 elseif t1 < (-pi/2) & t2 > (pi/2)
211     s11 = -1 .*s11;
212     branchcase1 = 2;
213 else
214     branchcase1 = 0;
215 end
216
217 if t3 > (pi/2) & t4 < (-pi/2)
218     s21 = -1 .*s21;
219     branchcase2 = 1;
220 elseif t3 < (-pi/2) & t4 > (pi/2)
221     s21 = -1 .*s21;
222     branchcase2 = 2;
223 else
224     branchcase2 = 0;
225 end
226 %% Extract the parameters
227 Q = (s11.^2 -s21.^2 +1) ./(2 .*s11);        % quadratic solution for R
228 R = Q +sqrt(Q.^2 -1);                       % Reflection coefficient
229 % if abs(R) > 1                               % Check/change:  |R| < 1
230 %     R = 1 ./ R;
231 % end
232 inverted = find(abs(R) > 1);
233 R(inverted) = 1 ./ R(inverted);
234
235 P = (s21) ./ (1 -R .*s11);          % 1-way phase delay-attenuation
236     kz = 1j .* log(P) ./ d;         %
237 z = (1 +R) ./ (1 -R);               % material impedence
```

```
238
239 mu_r = (z .*kz) ./kz0;                          % Relative permeability
240 eps_r = (kc.^2 + kz.^2) ./(k0.^2 .*mu_r);     % Relative permittivity
241 %% Uncertainty analysis
242 mu_fun = @(d_) (z .*(1j .* log(P) ./ d_)) ./kz0;
243 eps_fun = @(d_) (kc.^2 + (1j .* log(P) ./ d_).^2) ./(k0.^2 ...
       .*mu_fun(d_));
244 p_d = 1./(2*Δ_d);
245 Δ_t = abs(tempF - 69);       % assuming average room temperature at 69 F
246     if isequal(matl,'Alumina')  % set matl coefficient of thermal ...
           expansion
247         alpha = 4.7e-6;
248     elseif isequal(matl,'Ferrite')
249         alpha = 6.7e-6;
250     else
251         alpha = 0;
252     end
253 Δ_lt = alpha *Δ_t *d;    % change in length due to temperature
254 Δ_d = Δ_d + Δ_lt;    % combined measurement & thermal thickness ...
       uncertainty
255 sigma_d = Δ_d ./sqrt(3);     % discrete uniform distribution
256 d0 = d;
257 sigma_eps_pr = abs( real(eps_fun(d0+Δ_d) -eps_fun(d0)) /sqrt(3) );
258 sigma_eps_ppr = abs( imag(eps_fun(d0+Δ_d) -eps_fun(d0)) /sqrt(3) );
259 sigma_mu_pr = abs( real(mu_fun(d0+Δ_d) -mu_fun(d0)) /sqrt(3) );
260 sigma_mu_ppr = abs( imag(mu_fun(d0+Δ_d) -mu_fun(d0)) /sqrt(3) );
261 X = 2;
262 %% show the computed data
263 figure(2);
264     set(gcf,'units','normalized','position',[0 0 1 1])
265  subplot(2,2,1)
266         plot(freqG,real(s11n),'b-', freqG,imag(s11n),'b-.', ...
```

```
267                freqG,real(s21n),'m-', freqG,imag(s21n),'m-.')
268      xlabel('Frequency [GHz]'),     ylabel('S-Parameter')
269      title(['' num2str(tempF) ' F  DCHTWG De-embeded Normalized ...
             S-Parameters, Complex'])
270      axis square
271      legend('s_{11}^{Re}','s_{11}^{Im}','s_{21}^{Re}','s_{21}^{Im}',...
272                  'Location','eastoutside','FontSize',LFS)
273   subplot(2,2,2)
274      plot(freqG,abs(s11n),'b-', freqG,abs(s21n),'m--',...
275              freqG,abs(s12n),'c-', freqG,abs(s22n),'r--')
276      xlabel('Frequency [GHz]'),   ylabel('S-Parameter, Mag')
277      title(['' num2str(tempF) ' F  DCHTWG De-embeded Normalized ...
             S-Parameters, Magnitude'])
278      axis square
279      legend('|s_{11}|','|s_{21}|','|s_{12}|','|s_{22}|',...
280                  'Location','southeastoutside','FontSize',LFS)
281   subplot(2,2,4)
282      plot(freqG,unwrap(angle(s11n)),'b-', ...
             freqG,unwrap(angle(s21n)),'m--',...
283                freqG,unwrap(angle(s12n)),'c-', ...
                     freqG,unwrap(angle(s22n)),'r--')
284      xlabel('Frequency [GHz]'),   ylabel('S-Parameter, Phase ...
             [Radians/\pi]')
285      title(['' num2str(tempF) ' F  DCHTWG De-embeded Normalized ...
             S-Parameters, Phase'])
286      axis square
287      legend('\angle s_{11}','\angle s_{21}','\angle s_{12}','\angle ...
             s_{22}',...
288                  'Location','southeastoutside','FontSize',LFS)
289   figure(3);
290      set(gcf,'units','normalized','position',[0 0 1 1])
291    subplot(2,2,1)
```

```
292         plot(freqG,real(s11),'b-', freqG,imag(s11),'b-.', ...
293               freqG,real(s21),'m-', freqG,imag(s21),'m-.')
294     xlabel('Frequency [GHz]'),     ylabel('S-Parameter')
295     title(['' num2str(tempF) ' F  DCHTWG De-embeded S-Parameters, ...
           Complex'])
296     axis square
297     legend('s_{11}^{Re}','s_{11}^{Im}','s_{21}^{Re}','s_{21}^{Im}',...
298                 'Location','eastoutside','FontSize',LFS)
299  subplot(2,2,2)
300     plot(freqG,abs(s11),'b-', freqG,abs(s21),'m--')
301     xlabel('Frequency [GHz]'),   ylabel('S-Parameter, Mag')
302     title(['' num2str(tempF) ' F  DCHTWG De-embeded S-Parameters, ...
           Magnitude'])
303     axis square
304     legend('|s_{11}|','|s_{21}|','Location','southeastoutside','FontSize',LFS)
305  subplot(2,2,4)
306     plot(freqG,(t1+t2)/(2*pi),'b-',freqG,(t3+t4)/(2*pi),'m--')
307     xlabel('Frequency [GHz]'),   ylabel('S-Parameter, Phase ...
           [Radians/\pi]')
308     title(['' num2str(tempF) ' F  DCHTWG De-embeded S-Parameters, ...
           Phase'])
309     axis square
310     legend('\angle s_{11}','\angle ...
           s_{21}','Location','southeastoutside','FontSize',LFS)
311 %% show the computed material parameters
312 figure(4)
313     set(gcf,'units','normalized','position',[0.2 0.3 0.69 0.27])
314     set(gcf,'PaperPositionMode','auto')
315     plot(freqG, real(eps_r), 'b-', freqG, imag(eps_r), 'c--',...
316            freqG, real(mu_r), 'r-.', freqG, imag(mu_r), ...
                  'm:','LineWidth',2)
317     xlabel('Frequency [GHz]'), axis([8 12.5 0 14])
```

```
318     title(['' num2str(tempF) ' F DCHTWG ' matl ' Properties'])
319     legend('\epsilon_{r}^{Re}','\epsilon_{r}^{Im}',...
320             '\mu_{r}^{Re}','\mu_{r}^{Im}',...
321              'Location','eastoutside','FontSize',LFS)
322 savefig(char(strcat([mtd '_' matl '_' num2str(tempF) ...
       '_eps-mu'],'.fig')))
323 print(char(strcat([mtd '_' matl '_' num2str(tempF) ...
       '_eps-mu'])),'-djpeg')
324 %     X=2;
325     factor = 5; % to thin out the error bars
326     scale_index = (1:factor:size(freqG));
327 figure(5)
328     set(gcf,'units','normalized','position',[0.2 0.3 0.69 0.27])
329     set(gcf,'PaperPositionMode','auto')
330 errorbar(freqG(scale_index), real(eps_r(scale_index)),...
331     real(X*sigma_eps_pr(scale_index)),  'b-','LineWidth',2), hold on
332 errorbar(freqG(scale_index), imag(eps_r(scale_index)),...
333     imag(X*sigma_eps_ppr(scale_index)), 'c--','LineWidth',2)
334 errorbar(freqG(scale_index), real(mu_r(scale_index)),...
335     real(X*sigma_mu_pr(scale_index)), 'r-.','LineWidth',2)
336 errorbar(freqG(scale_index), imag(mu_r(scale_index)),...
337     imag(X*sigma_mu_ppr(scale_index)), 'm:','LineWidth',2), hold off
338 %     plot(freqG, real(eps_r), 'b-', freqG, imag(eps_r), 'c-.',...
339 %             freqG, real(mu_r), 'r-', freqG, imag(mu_r), 'm-')
340     xlabel('Frequency [GHz]'), axis([8 12.5 0 14])
341     title(['' num2str(tempF) ' F DCHTWG ' matl ' Properties'])
342     legend('\epsilon_{r}^{Re}','\epsilon_{r}^{Im}',...
343             '\mu_{r}^{Re}','\mu_{r}^{Im}',...
344              'Location','eastoutside','FontSize',LFS)
345 savefig(char(strcat([mtd '_' matl '_' num2str(tempF) ...
       '_eps-mu_err'],'.fig')))
346 print(char( strcat([mtd '_' matl '_' num2str(tempF) '_eps-mu_err']) ...
```

```
    ),'-djpeg')
%% save data for export and comparison
    savefile = ['' file '.mat'];
%     savefile = ['' matl '_' num2str(tempF) '.mat'];
save(savefile,'freqG','eps_r','sigma_eps_pr','sigma_eps_ppr','mu_r',...
    'sigma_mu_pr','sigma_mu_ppr','tempF','matl','mtd','X','scale_index')
%% S-parameter comp
figure
    plot(freqG,abs(s11me),freqG,angle(s11me),...
        freqG,abs(s21me),freqG,angle(s21me))
    xlabel('Frequency [GHz]')
    hold on
    plot(freqG,abs(s11ms),freqG,angle(s11ms),...
        freqG,abs(s21ms),freqG,angle(s21ms))
    legend('s11me mag','s11me phase','s21me mag','s21me phase',...
        's11ms mag','s11ms phase','s21ms mag','s21ms phase')
```

Appendix B. NRW Deliverable Code

```
%% Network Analyzer data processing, NRW technique, Capt Jeff Sovern
% Thesis code
clc,  clear, close all
LFS = 10;       % legend font size
mtd = 'NRW';
%%  Input the material data
N = input('How many data runs to analyze? [#] ');   % statistical runs
numpts = 201;
%% Load the data
% set variables
freq = zeros(numpts,N);
s11m = zeros(numpts,N);
s21m = zeros(numpts,N);
s12m = zeros(numpts,N);
s22m = zeros(numpts,N);
for n = 1:N;
% Load the data files
   disp(['Select the calibrated data file... '])
[filename, pathname] = uigetfile( ...
{'*.cti;*.xls;*.txt;*.s2p','Network Analyzer Data';...
'*.m;*.fig;*.mat;*.slx;*.mdl','MATLAB Files ...
    (*.m,*.fig,*.mat,*.slx,*.mdl)';
   '*.xls','Excel files (*.xls)'; ...
   '*.m',  'Code files (*.m)'; ...
   '*.mat','MAT-files (*.mat)'; ...
   '*.*',  'All Files (*.*)'}, ...
   'Pick a file');
if isequal(filename,0)
   disp('User selected Cancel')
```

```
29 else
30    disp(['User selected calibration file: ', fullfile(pathname, ...
         filename)])
31    [pn,file,extension] = fileparts(filename);
32 end
33 % Load the network analyzer calibration data
34 if isequal(extension,'.cti')
35     [freq(:,n),s11m(:,n),s21m(:,n),s12m(:,n),s22m(:,n)] = ...
          cti_data_load2(filename);
36 elseif isequal(extension,'.s2p')
37     [freq(:,n),s11m(:,n),s21m(:,n),s12m(:,n),s22m(:,n)] = ...
          s2p_data_load(filename);
38 elseif isequal(extension,'.xls')
39     [freq(:,n),s11m(:,n),s21m(:,n),s12m(:,n),s22m(:,n)] = ...
          xls_data_load(filename);
40 end
41 freqG(:,n) = freq(:,n) / 1e9;      % Frequency [GHz]
42 end
43 % pull the stats out
44 freqstd = std(freq,0,2);
45 freqGstd = std(freqG,0,2);
46 s11mstd = std(s11m,0,2);
47 s21mstd = std(s21m,0,2);
48 s12mstd = std(s12m,0,2);
49 s22mstd = std(s22m,0,2);
50
51 freqbar = mean(freq,2);
52 freqGbar = mean(freqG,2);
53 s11mbar = mean(s11m,2);
54 s21mbar = mean(s21m,2);
55 s12mbar = mean(s12m,2);
56 s22mbar = mean(s22m,2);
```

```
57 %%  Input the material data
58 tempF = input('What is the temperature of the collection? ( F ) ');
59 matl = input('What material is loaded in the waveguide? (if nothing ...
       type air) ','s');
60 % Alumina sample: 1.957mm
61 % Mica Sample material Thickness: 3.23mm0.01
62 % Magram FGM125 Sample material Thickness: 3.17mm0.02
63 % White Sample material Thickness: 4.13mm
64 % research sample holder thicknes: 9.73 mm0.01
65 % sample holder thicknes: 9.66 mm
66 % insert length: 152.50 mm
67 d = 1e-3 * input('What is the material thickness? [mm] ');
68 Δ_d = 1e-3 * input('     What is the material thickness variance? ...
       [mm] ');
69 %%  Input the waveguide data
70 a = 22.86e-3;    b = 10.16e-3; % wr-90 x-band, 0.9" x 0.4" [m]
71 eps0 = 8.854187817e-12; % vacuum permittivity [F/m]
72 mu0 = pi * 4e-7;         % vacuum permeability [F/m]
73 c = 299792458;           % light speed [m/s]
74 omega = 2*pi .* freq;    % angular frequency [rad/s]
75 k0 = omega ./ c;         % freespace wavenumber
76 kc = pi/a;               % TE10 mode
77 kz0 = sqrt(k0 .^2 - kc .^2);     %
78 lh = 1e-3 * input('What is the sample holder thickness? [mm] ');
79 lh_Δ = 1e-3 * input('     What is the sample holder thickness ...
       variance? [mm] ');
80 lpd = 1e-3 * input('What is the sample placement depth? [mm] ');
81 % lpd_Δ = 1e-3 * input('     What is the sample placement variance? ...
       [mm] ');
82 lb = lh - d;             % port 2 side air gap of the material in holder
83 %% show the raw data
84 figure(1);
```

```
subplot(1,2,1)
    plot(freqGbar,real(s11mbar),'b-', freqGbar,imag(s11mbar),'b-.',...
          freqGbar,real(s21mbar),'m-', freqGbar,imag(s21mbar),'m-.',...
           freqGbar,real(s12mbar),'y--', ...
              freqGbar,imag(s12mbar),'y--.',...
            freqGbar,real(s22mbar),'c--', freqGbar,imag(s22mbar),'c--.')
    xlabel('Frequency [GHz]'),     ylabel('S-Parameter')
    title('NRW Raw S-Parameters, Complex')
    axis square
    legend('s_{11}^{Re}','s_{11}^{Im}','s_{21}^{Re}','s_{21}^{Im}',...
            's_{12}^{Re}','s_{12}^{Im}','s_{22}^{Re}','s_{22}^{Im}',...
                'Location','eastoutside','FontSize',LFS)
subplot(1,2,2)
    plot(freqGbar,abs(s11mbar),'b-',...
          freqGbar,abs(s21mbar),'m-',...
           freqGbar,abs(s12mbar),'y--',...
            freqGbar,abs(s22mbar),'c--')
    xlabel('Frequency [GHz]'),     ylabel('S-Parameter')
    title('NRW Raw S-Parameters, Magnitude')
    axis square
    legend('|s_{11}|','|s_{21}|',...
            '|s_{12}|','|s_{22}|',...
                'Location','eastoutside','FontSize',LFS)
%% De-embed Technique #1 (no additional waveguide, material present)
    s11 = s11m .* exp(2j * kz0 * lpd);
    s21 = s21m .* exp(j * kz0 * (lpd + lb));
    s12 = s12m .* exp(j * kz0 * (lpd + lb));
    s22 = s22m .* exp(2j * kz0 * lb);
%% Root test
t1 = unwrap(angle(s11) );
t2 = unwrap(angle(s21) );
t3 = unwrap(angle(s12) );
```

```
116 t4 = unwrap(angle(s22) );
117 if t1 > (pi/2) & t2 < (-pi/2)
118     s11 = -s11;
119 elseif t1 < (-pi/2) & t2 > (pi/2)
120     s11 = -s11;
121 end
122 if t3 > (pi/2) & t4 < (-pi/2)
123     s21 = -s21;
124 elseif t3 < (-pi/2) & t4 > (pi/2)
125     s21 = -s21;
126 end
127 % pull the stats out
128 s11std = std(s11,0,2);
129 s21std = std(s21,0,2);
130 s12std = std(s12,0,2);
131 s22std = std(s22,0,2);
132
133 s11bar = mean(s11,2);
134 s21bar = mean(s21,2);
135 s12bar = mean(s12,2);
136 s22bar = mean(s22,2);
137 %% Extract the material properties
138 Q = ( s11 .^2 - s21 .^2 + 1 ) ./ ( 2 .* s11 );
139 R = Q + sqrt(Q .^2 - 1);
140 % if abs(R) > 1
141 %     R = 1 ./ R;
142 % end
143 inverted = find(abs(R) > 1);
144 R(inverted) = 1 ./ R(inverted);
145     P = (s21) ./ (1 - R .* s11);
146         kz = 1j .* log(P) ./ d;
147     z = (1 + R) ./ (1 - R);
```

```
mu_r = (z .* kz) ./ kz0;                              % Relative permeability
eps_r = ( kc .^2 + kz .^2 ) ./ (k0 .^2 .* mu_r); % Relative permittivity
% pull the stats out
mu_r_std = std(mu_r,0,2);
eps_r_std = std(eps_r,0,2);
mu_r = mean(mu_r,2);
eps_r = mean(eps_r,2);
%% Uncertainty analysis
mu_fun = @(d_) (z .*(1j .* log(P) ./ d_)) ./kz0;
eps_fun = @(d_) (kc.^2 + (1j .* log(P) ./ d_).^2) ./(k0.^2 ...
    .*mu_fun(d_));
p_d = 1./(2*Δ_d);
Δ_t = abs(tempF - 69);       % assuming average room temp at 69 F
    if isequal(matl,'Alumina')  % set matl coefficient of thermal ...
        expansion
        alpha = 4.7e-6;
    elseif isequal(matl,'Ferrite')
        alpha = 6.7e-6;
    else
        alpha = 0;
    end
Δ_lt = alpha *Δ_t *d;   % change in length due to temperature
Δ_d = Δ_d + Δ_lt;   % combined measurement & thermal thickness ...
    uncertainty
sigma_d = Δ_d ./sqrt(3);    % discrete uniform distribution
d0 = d;
sigma_eps_pr = abs( real(eps_fun(d0+Δ_d) -eps_fun(d0)) /sqrt(3) );
sigma_eps_ppr = abs( imag(eps_fun(d0+Δ_d) -eps_fun(d0)) /sqrt(3) );
sigma_mu_pr = abs( real(mu_fun(d0+Δ_d) -mu_fun(d0)) /sqrt(3) );
sigma_mu_ppr = abs( imag(mu_fun(d0+Δ_d) -mu_fun(d0)) /sqrt(3) );
X = 2;
%% show the computed data
```

```
figure(2);
subplot(1,2,1)
    plot(freqGbar,real(s11bar),'b-', freqGbar,imag(s11bar),'b-.', ...
            freqGbar,real(s21bar),'m-', freqGbar,imag(s21bar),'m-.',...
             freqGbar,real(s12bar),'y--', ...
                freqGbar,imag(s12bar),'y--.',...
              freqGbar,real(s22bar),'c--', freqGbar,imag(s22bar),'c--.')
    xlabel('Frequency [GHz]'),     ylabel('S-Parameter')
    title('NRW De-embeded S-Parameters, Complex')
    axis square
    legend('s_{11}^{Re}','s_{11}^{Im}','s_{21}^{Re}','s_{21}^{Im}',...
            's_{12}^{Re}','s_{12}^{Im}','s_{22}^{Re}','s_{22}^{Im}',...
                'Location','eastoutside','FontSize',LFS)
subplot(1,2,2)
    plot(freqGbar,abs(s11bar),'b-',...
          freqGbar,abs(s21bar),'m-',...
           freqGbar,abs(s12bar),'y--',...
            freqGbar,abs(s22bar),'c--')
    xlabel('Frequency [GHz]'),     ylabel('S-Parameter')
    title('NRW De-embeded S-Parameters, Magnitude')
    axis square
    legend('|s_{11}|','|s_{21}|',...
            '|s_{12}|','|s_{22}|',...
                'Location','eastoutside','FontSize',LFS)
    factor = 5; % to thin out the error bars
    scale_index = (1:factor:size(freqG));
figure(3)
    set(gcf,'units','normalized','position',[0.2 0.3 0.69 0.27])
    set(gcf,'PaperPositionMode','auto')
errorbar(freqGbar, real(eps_r),...
    X*(real(eps_r_std)+mean(sigma_eps_pr,2)),  'b-'), hold on
errorbar(freqGbar, imag(eps_r),...
```

```
208     X*(imag(eps_r_std)+mean(sigma_eps_ppr,2)), 'c--')
209 errorbar(freqGbar, real(mu_r),...
210     X*(real(mu_r_std)+mean(sigma_mu_pr,2)), 'r-.')
211 errorbar(freqGbar, imag(mu_r),...
212     X*(imag(mu_r_std)+mean(sigma_mu_ppr,2)), 'm:'), hold off
213 %     plot(freqG, real(eps_r), 'b-', freqG, imag(eps_r), 'c-.',...
214 %             freqG, real(mu_r), 'r-', freqG, imag(mu_r), 'm-')
215     xlabel('Frequency [GHz]')
216     title(['' num2str(tempF) ' F NRW ' matl ' Properties'])
217     legend('\epsilon_{r}^{Re}','\epsilon_{r}^{Im}',...
218            '\mu_{r}^{Re}','\mu_{r}^{Im}',...
219             'Location','eastoutside','FontSize',LFS)
220 %% save data for export and comparison
221     savefile = ['' file '.mat'];
222 %     savefile = ['' matl '_' num2str(tempF) '.mat'];
223 save(savefile,'freqG','eps_r','sigma_eps_pr','sigma_eps_ppr','mu_r',...
224     'sigma_mu_pr','sigma_mu_ppr','tempF','matl','mtd','X','scale_index')
```

Appendix C. Data Load Deliverable Code

```
function [freq,s11me,s12me,s21me,s22me,s11ms,s12ms,s21ms,s22ms] = ...
    cti_data_load4(filename);
% 4-port Network Analyzer data (.cti) load function
%% Load the network analyzer data
fileID = fopen(filename);
formatSpec1 = '%s %q %s %s';
h = textscan(fileID,formatSpec1,9,'HeaderLines',5,'Delimiter',' '); ...
    % header info
datapts = str2double(h{1,4}(1,1));      % how many data points collected
formatSpec2 = '%f32 %f32';
freq = cell2mat(textscan(fileID,'%f','HeaderLines',2)); % ...
    frequencies recorded
     s11a = textscan(fileID,formatSpec2,'HeaderLines',2,'Delimiter',',');
     s12a = textscan(fileID,formatSpec2,'HeaderLines',2,'Delimiter',',');
     s21a = textscan(fileID,formatSpec2,'HeaderLines',2,'Delimiter',',');
     s22a = textscan(fileID,formatSpec2,'HeaderLines',2,'Delimiter',',');
     s33a = textscan(fileID,formatSpec2,'HeaderLines',2,'Delimiter',',');
     s34a = textscan(fileID,formatSpec2,'HeaderLines',2,'Delimiter',',');
     s43a = textscan(fileID,formatSpec2,'HeaderLines',2,'Delimiter',',');
     s44a = textscan(fileID,formatSpec2,'HeaderLines',2,'Delimiter',',');
fclose(fileID);
% empty waveguide S-parameters
s11mr = s11a{1};    s11mi = s11a{2};    % measured real & imaginary ...
    S-param
     s11me = complex(s11mr,s11mi);       % complex pair
s12mr = s12a{1};    s12mi = s12a{2};
     s12me = complex(s12mr,s12mi);
s21mr = s21a{1};    s21mi = s21a{2};
     s21me = complex(s21mr,s21mi);
```

```
26 s22mr = s22a{1};    s22mi = s22a{2};
27     s22me = complex(s22mr,s22mi);
28 % sample loaded waveguide S-parameters
29 s33mr = s33a{1};    s33mi = s33a{2};    % measured real & imaginary ...
       S-param
30     s11ms = complex(s33mr,s33mi);       % complex pair
31 s34mr = s34a{1};    s34mi = s34a{2};
32     s12ms = complex(s34mr,s34mi);
33 s43mr = s43a{1};    s43mi = s43a{2};
34     s21ms = complex(s43mr,s43mi);
35 s44mr = s44a{1};    s44mi = s44a{2};
36     s22ms = complex(s44mr,s44mi);
37 end
```

Bibliography

1. L. F. Chen, C. K. Ong, C. P. Neo, V. V. Varadan, and V. K. Varadan, *Microwave Electronics: Measurement and Materials Characterization*. John Wiley & Sons, 2004, vol. 19, Ch. 12.

2. C. Larsson, D. Sjöberg, and D. Sjöberg, "High temperature waveguide measurements of the permittivity and permeability," in *ICECom, 2010 Conference Proceedings*, 2010, pp. 1–4.

3. C. A. Balanis, *Advanced Engineering Electromagnetics*, 2nd ed. John Wiley & Sons, 2012, Ch. 2.2.

4. J. Baker-Jarvis, E. J. Vanzura, and W. A. Kissick, "Improved Technique for Determining Complex Permittivity with the Transmission/Reflection Method," *IEEE Transactions on Microwave Theory and Techniques*, vol. 38, no. 8, pp. 1096–1103, 1990.

5. M. Aral, J. G. P. Binner, G. E. Carr, and T. E. Cross, "High Temperature Dielectric Measurements on Ceramics," *MRS Proceedings*, p. 611, Feb. 1992.

6. W. W. Ho, "High-temperature dielectric properties of polycrystalline ceramics," *MRS Proceedings*, pp. 137–148, Jan. 1988.

7. W. Tinga, "Rapid High Temperature Measurement of Microwave Dielectric Properties," *MRS Proceedings*, p. 505, Feb. 1992.

8. J. A. Batt, R. Rukus, and M. Gilden, "General Purpose High Temperature Microwave Measurement of Electromagnetic Properties," *Material Research Society Proceedings*, no. Symposium L Microwave Processing of Materials III, pp. 553–559.

9. M. M. N. Afsar, J. R. J. Birch, R. N. Clarke, and G. Chantry, "The Measurement of the Properties of Materials," *Proceedings of the IEEE*, vol. 74, no. 1, pp. 183–199, 1986.

10. V. V. Varadan, V. K. Varadan, R. D. Hollinger, and D. K. Ghodgaonkar, "Free-space, broadband measurements of high-temperature, complex dielectric properties at microwave frequencies," *IEEE Transactions on Instrumentation and Measurement*, no. 5, pp. 842–846.

11. A. M. Nicolson and G. F. Ross, "Measurement of the Intrinsic Properties of Materials by Time-Domain Techniques," *Instrumentation and Measurement, IEEE Transactions on*, vol. 19, no. 4, pp. 377–382, 1970.

12. G. W. Hanson, J. M. Grimm, and D. P. Nyquist, "An improved de-embedding technique for the measurement of the complex constitutive parameters of materials using a stripline field applicator," *Instrumentation and Measurement, IEEE Transactions on*, vol. 42, no. 3, pp. 740–745, 1993.

13. E. A. Buschelman, M. J. Havrilla, A. J. Terzuoli, and P. E. Crittenden, "Material Characterization Improvement in High Temperature Rectangular Waveguide Measurements," in *International Conference on Electromagnetics in Advanced Applications, 2007.*

14. W. B. Weir, "Automatic measurement of complex dielectric constant and permeability at microwave frequencies," *Proceedings of the IEEE*, vol. 62, no. 1, pp. 33–36, 1974.

15. J. S. Sovern, M. J. Havrilla, and M. W. Hyde, "Electromagnetic characterization of materials using a dual chambered high temperature waveguide," in *USNC-URSI National Radio Science Meeting (NRSM), 2016.*, Jan. 2016.

16. *Haynes ® 230 ® alloy*, Haynes International High-temperature alloys, Oct 2015. [Online]. Available: http://www.haynesintl.com/

17. *ECCOSORB FGM-125 Thin, flexible, broadband, microwave absorber*, Emerson & Cuming Microwave Products, Sep 2014.

18. *AD-998 ALUMINA MATERIAL PROPERTIES*, CoorsTek Technical Ceramics, Dec 2015. [Online]. Available: http://www.coorstek.com/materials/ceramics/alumina_ad-998.php

19. Agilent, "Agilent Network Analyzer Basics," *Analysis*, pp. 1–94.

20. F. P. Beer, E. R. Johnston Jr., and J. T. DeWolf, *Mechanics of Materials*, 3rd ed. McGraw-Hill, 2002, Ch. 2.

REPORT DOCUMENTATION PAGE

Form Approved
OMB No. 0704–0188

1. REPORT DATE *(DD–MM–YYYY)*	2. REPORT TYPE	3. DATES COVERED *(From — To)*
24–03–2016	Master's Thesis	Sept 2014 — Mar 2016

4. TITLE AND SUBTITLE

Electromagnetic Characterization of Materials Using a Dual Chambered High Temperature Waveguide

5a. CONTRACT NUMBER

5b. GRANT NUMBER

5c. PROGRAM ELEMENT NUMBER

6. AUTHOR(S)

Sovern, Jeffrey S., Capt, USAF

5d. PROJECT NUMBER

16G118

5e. TASK NUMBER

5f. WORK UNIT NUMBER

7. PERFORMING ORGANIZATION NAME(S) AND ADDRESS(ES)

Air Force Institute of Technology
Graduate School of Engineering and Management (AFIT/EN)
2950 Hobson Way
WPAFB OH 45433-7765

8. PERFORMING ORGANIZATION REPORT NUMBER

AFIT-ENG-MS-16-M-047

9. SPONSORING / MONITORING AGENCY NAME(S) AND ADDRESS(ES)

Air Force Research Laboratory, Sensors Directorate
Attn: Garrett J. Stenholm
2591 K Street, Bldg 254
WPAFB OH 45433-7765
DSN 785-9179, COMM 937-255-9179
Email: garrett.stenholm@us.af.mil

10. SPONSOR/MONITOR'S ACRONYM(S)

AFRL/RYS

11. SPONSOR/MONITOR'S REPORT NUMBER(S)

12. DISTRIBUTION / AVAILABILITY STATEMENT

DISTRIBUTION STATEMENT A:
APPROVED FOR PUBLIC RELEASE; DISTRIBUTION UNLIMITED.

13. SUPPLEMENTARY NOTES

This material is declared a work of the U.S. Government and is not subject to copyright protection in the United States.

14. ABSTRACT Current high-temperature electromagnetic material characterization is a time consuming process that typically requires three days to collect data from one material specimen. The standard high-temperature process involving rectangular waveguides requires measurements of the sample, the empty waveguide, and a metal short standard completed in separate heated runs over three days. The technique developed here will reduce the measurement process from three days down to just one day. The research uses a position independent approach for isotropic materials for effective transmission and reflection parameters; eliminating the need for a metal short and one measurement day. A new dual chambered waveguide design will reduce measurement time down to just one day through simultaneous measurement of the sample and the empty second chamber. A vector network analyzer (VNA) will be used to run X-band data collects at incrementally increasing temperatures up to approximately $1000°F$. Results will be the test material's permittivity and permeability as calculated from the Nicolson-Ross-Weir inversion algorithm for computing permittivity and permeability using VNA measured S-parameters at increasing temperatures.

15. SUBJECT TERMS

electromagnetism, X-Band, material characterization, material measurement, MATLAB®, network analyzer, high temperature

16. SECURITY CLASSIFICATION OF:			17. LIMITATION OF ABSTRACT	18. NUMBER OF PAGES	19a. NAME OF RESPONSIBLE PERSON
a. REPORT	b. ABSTRACT	c. THIS PAGE			Dr. Michael J. Havrilla, AFIT/ENG
U	U	U	UU	75	19b. TELEPHONE NUMBER *(include area code)* (937) 255-3636, x4582; michael.havrilla@afit.edu